Fire-induced ceiling jet characteristics in tunnels under different ventilation conditions

Ying Zhen Li, Haukur Ingason

BRANDFORSK Project 306-131

SP Technical Research Institute of Sweden

Fire Research

SP Report 2015:23

Fire-induced ceiling jet characteristics in tunnels under different ventilation conditions

Ying Zhen Li, Haukur Ingason

Abstract

Fire-induced ceiling jet characteristics in tunnels under different ventilation conditions

Theoretical analyses and experiments were conducted to investigate the ceiling jet characteristics in tunnel fires. A series of fire tests was carried out in two model tunnels with a scaling ratio of 1:10, with varying heat release rates, ventilation velocities, fire source heights and tunnel geometries. The key parameters investigated include flame length, ceiling jet velocity, ceiling jet mass flow rate, ceiling jet temperature distribution, radiation heat flux and fire spread were analysed and correlations for these parameters are proposed. Theoretical and experimental data are compared and evaluated. The results show a very good agreement between the test data and the proposed theoretical models.

Key words: model scale, tunnel fire, ceiling jet, flame length, gas velocity, smoke flow rate, gas temperature, radiation, fire spread

SP Sveriges Tekniska Forskningsinstitut
SP Technical Research Institute of Sweden

SP Report 2015:23
ISBN 978-91-88001-53-5
ISSN 0284-5172
Borås

Contents

Preface

This project was funded by the Swedish Fire Research Board (BRANDFORSK) which is greatly acknowledged. This project was also financially supported by SP internal funding.

The technicians Michael Magnusson, Sven-Gunnar Gustafsson, Niklas Brude, Henrik Fredriksson, Tarmo Karjalainen, Emil Norberg, Lars Gustavsson and Morgan Lehtinen at SP Fire Research are acknowledged for the construction of the test rig and the assistance during performance of the tests. Thanks also to Prof. Michael Försth at SP Fire Research for the valuable comments.

Summary

Theoretical analyses and experimental work were carried out to investigate the ceiling jet characteristics in tunnel fires. The key ceiling jet characteristic parameters focused on are flame lengths, ceiling jet velocity, ceiling jet mass flow rate, gas temperatures, radiation and fire spread. A series of fire tests was carried out in two model tunnels with a scaling ratio of 1:10. The parameters tested include heat release rate, ventilation velocity, fire source height and tunnel geometry.

A theoretical model of flame lengths in tunnels is proposed and validated using test data. Under low ventilation, i.e. the dimensionless velocity u^*<0.3, there exists both upstream flame and downstream flame, and the upstream flame length decreases linearly with the increasing velocity. Under high ventilation, i.e. u^*>0.3, only downstream flame exists. Regardless of ventilation velocity, the downstream flame length increases linearly with the heat release rate, and decreases with tunnel width and effective tunnel height. The total flame length, i.e. the sum of downstream and upstream flame lengths, can be as long as twice the downstream flame lengths. Correlations for downstream flame lengths, upstream flame lengths, and total flame lengths are proposed.

Theoretical model of ceiling jet velocity in tunnels under different ventilation conditions is proposed and validated using test data. Under natural ventilation, the ceiling jet velocity increases with heat release rate and decreases with effective tunnel height. Under forced ventilation, the ceiling jet velocity increases with the ventilation velocity and the ceiling jet temperature.

The mass flow rate of the fire plume increases with heat release rate and effective tunnel height, under natural ventilation. Under high ventilation, the smoke mass flow rate increases linearly with ventilation velocity, independent of heat release rate.

Theoretical analysis of distribution of gas temperature of the ceiling jet in a tunnel fire is presented. It has been found that there are virtual origins for large tunnel fires and the gas temperatures between the fire source center and the virtual origin decrease very slowly. This is due to the large amount of heat released within the ceiling intensive combustion region. Correlations for both the ceiling gas temperatures and the virtual origins under low and high ventilation are proposed.

Theoretical models of radiation heat fluxes in small and large tunnel fires are presented and verified using test data. The tunnel surfaces in the upper smoke layer are exposed to smoky gases and/or flames in a large fire. The incident heat flux in the upper smoke layer can be simply correlated with the smoke temperature and the emissivity of the smoke volume. For large fires, the emissivity can be assumed to be 1. To calculate the incident heat flux in the lower layer, the view factor must be accounted for, together with the upper layer smoke temperature and the emissivity of the smoke volume.

Fire spread to targets on the floor level or at a certain height above floor occurred when the radiation heat flux is greater than approximately 20 kW/m^2. The net heat flux on the fuel surface at the ignition is found to be a positive value.

1 Introduction

Numerous catastrophic tunnel fires occurred in the past decades have forced us to rethink the fire safety issues in tunnels. In the Mont Blanc tunnel fire in 1999, a total of 26 vehicles on the French side and 8 lorries on the Italian side caught fire. The corresponding total flame length was about 700 m [1]. In the Tauern tunnel fire in Austria in 1999, the flame was estimated to be as long as about 300 m and the ceiling was damaged over a total length of 350 m [1]. These fire accidents showed that the flame lengths in these catastrophic tunnel fires were much longer and the fire spread to the neighbouring vehicles were much more serious than what was expected. These fires became eye-openers for engineers and scientists, but profound and systematic knowledge about how to estimate these long flames is still lacking. Even in some small tunnel fires, both the smoke de-stratification and the toxic gases released threaten people’s lives. To avoid these catastrophic accidents and reduce the loss in the future, we need to clearly understand the mechanism of the ceiling jet characteristics and the resulting fire spread.

Figure 1 and Figure 2 show how the smoke spreads in a small tunnel fire under natural ventilation and high ventilation, respectively. The fire-induced smoke plume impinges on the ceiling and travels along the ceiling. The smoke flows entrains the fresh air flow from lower layer as they travel along the ceiling. The total smoke flow rate increases gradually until the smoke descends to the floor level when the stratification disappears.

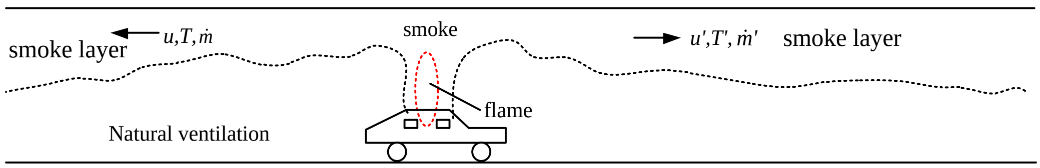

Figure 1 Smoke spread in a small tunnel fire under low ventilation or natural ventilation.

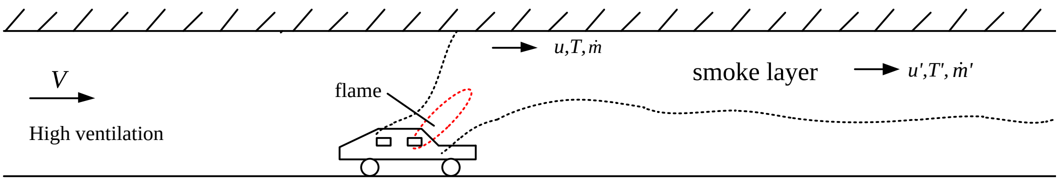

Figure 2 Smoke spread in a small tunnel fire under high ventilation.

In a large tunnel fire, the flame impinges on the tunnel ceiling and extends a significant distance along the ceiling. The behaviour of smoke, flames and ceiling jets are dependent on the ventilation conditions. The ceiling flame jets and the smoke layer under low ventilation and high ventilation are shown in Figure 3 and Figure 4, respectively. Note that in a large tunnel fire, the ceiling jets nearby the fire is characteristic of the flame jets. Under low ventilation, the flame extends in two directions while under high ventilation exists only in one direction. Due to confinement of tunnel walls in a tunnel fire, the horizontal flame length of a tunnel fire becomes much longer compared to an enclosure fire where the flames extend axisymmetric and radially. This results in an increased risk of fire spread to the neighboring objects or vehicles due to the high radiation from the flame, especially when there are queues in a road tunnel. This is one of the key issues in the motivation for whether we need or not to install a water spray system in a tunnel. The fire spread sharply increases the total fire size and results in longer flame length and higher radiation far away from the fire, thus involving more vehicles. This phenomena was observed in the Mont Blanc tunnel fires and in Tauern tunnel fires [1] but has not been systematically investigated in tunnel fires. The investigation of the ceiling jets will improve our understanding of the mechanism of the ceiling flame combustion, flame length and fire spread to neighbouring targets. Further, it will provide the initial conditions for further smoke movement along the tunnel.

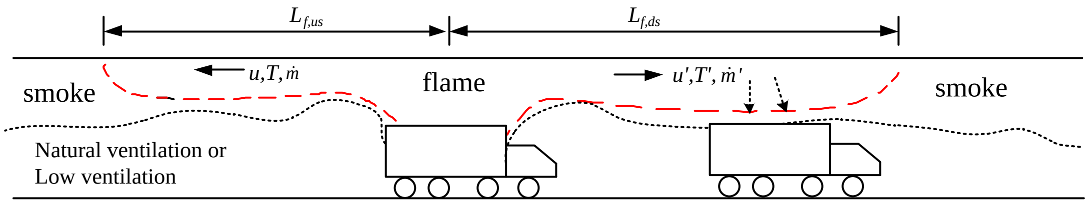

Figure 3 Ceiling flame in a large tunnel fire under low ventilation or natural ventilation.

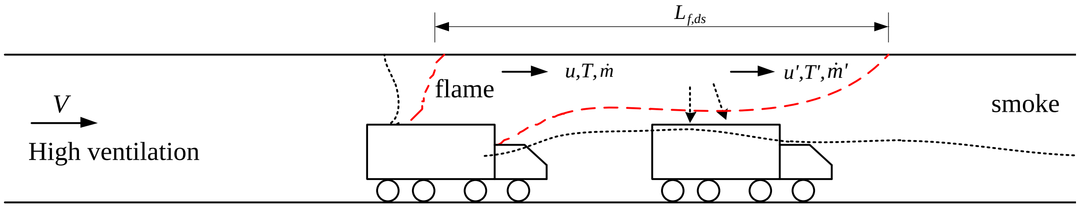

Figure 4 Ceiling flame in a large tunnel fire under high ventilation.

The investigation of ceiling jet characteristics will give us valuable information about the flame length and the possible fire spread. These characteristic parameters indicate the hazards of any given tunnel fire, and are the key parameters in the design of a tunnel fire safety system.

2 State-of-the-art research

In the past decades, research on tunnel fire has mainly focused on design fires [2-4] and smoke control in longitudinally ventilated tunnels [5-7].

There is a clear lack of research on detailed ceiling jet characteristics in tunnel fires. Note that in open fires, we can easily use established equations to calculate the flame height, gas temperature and gas velocity as a function of height. However, in tunnel fires, we cannot find similar tools to estimate these key parameters, with the exception of the maximum gas temperatures beneath the ceiling where much research has been conducted by Li et al. [8-10] based on both theory and model-scale and full-scale tests data. In the following, a short review of the individual topics is presented.

2.1 Flame length

Limited research has been carried out on the flame length in a large tunnel fire. Rew and Deaves [11] presented a flame length model for tunnel fires, which included heat release rate and longitudinal velocity. However, neither tunnel width nor tunnel height was considered. Their research was based on the investigation of the Channel Tunnel Fire in 1996 and test data from the HGV-EUREKA 499 fire test [12] and the Memorial Tests [13]. The equation is a conservative fit to a limited data obtained from the HGV-EUREKA 499 test. The weakness of the proposed equation is that no geometrical parameter has been taken into account, which makes it impossible to predict the flame length for other tunnels with different geometries. Lönnermark and Ingason [14] investigated the flame lengths from the Runehamar tests and used Alpert's equation [15] for ceiling jet temperatures to estimate the form of equation for flame length, and determined the uncertain coefficients by regression analysis. However, the tunnel ceiling is confined and thus the equation proposed by Alpert [15] may not be appropriate for large tunnel fires. Ingason and Li [16] presented a dimensionless equation to estimate the flame lengths under high ventilation. However, the flame lengths under low ventilation have not yet been investigated. Moreover, a theory needs to be proposed to clarify the correlation between ceiling flame combustion and flame length.

2.2 Ceiling jet velocity

The ceiling jets in ordinary building enclosure fires have been investigated by Alpert [15] and Heskestad et al. [17]. However, the ceiling jets in tunnel fires, especially in longitudinally ventilated tunnel fires, is completely different with those in room fires. Hinkley [18] proposed an equation to estimate the gas velocity for small corridor fires, however, it is based on a simple assumption of constant Richardson number which is not suitable for the momentum dominant ceiling jet flows in tunnel fires. Li et al. [19] analyzed the ceiling jet flows for small corridor fires. However, no entrainment was considered for the ceiling jets and the Reynolds' analogy was misused since in reality the convective heat flux rather than total heat flux should be used in the analogy.

2.3 Ceiling jet flow rate

Li et al. [8] proposed an equation to estimate the smoke flow rate at a certain height in a small fire under ventilation. This should be equivalent to the initial ceiling jet flow rate. However, the equation was only validated using the temperature data. Data of the initial ceiling gas flow rate are needed to validate this equation. Further, this equation could not be suitable for the strong flame plume.

2.4 Ceiling jet temperature

Li et al. [8-10, 20] have theoretically and experimentally investigated the maximum ceiling gas temperature and its corresponding position in tunnel fires and robust equations have been proposed for both low ventilation and high ventilation. However, how the flame temperature varies with distance in the vicinity of the fire has not yet been fully explored. Ingason and Li [16] found that while correlating all the temperature distribution curve, there is a “virtual origin” along the ceiling. The horizontal distance at the ceiling between the fire source and virtual origin needs to be clearly determined.

2.5 Ceiling jet radiation

Ingason et al. [21] investigated the radiation from the ceiling flame to the tunnel structure in the Runehemar tunnel fire tests. Ingason and Li [22] also found that there is a strong correlation between the ceiling gas temperature and the heat flux at the floor level in the far-field of the fire. However, the radiation directly from the flame to the objects at floor level or at a certain height in the vicinity of the fire needs to be thoroughly investigated, since the fire spread to the neighbouring objects or vehicles mainly results from this radiation.

2.6 Fire spread

Limited research has been carried out on the fire spread in a tunnel fire. Newman and Tewarson [23] argued that in duct flow the material at a location will ignite when the average temperature of the tunnel flow at this position has obtained a critical value. Lönnermark and Ingason [14] tested and investigated the fire spread in full scale tunnel fires and the results show that an average temperature of approximately 500 ºC seems to give the best correlation with fire spread. However, the data are rather limited. All the above work is based on the assumption of one-dimensional flow, however generally there is a strong stratification in the vicinity of the fire where the fire spread potentially occurs. Furthermore, the assumption of one-dimensional flow is completely invalid under low ventilation. Ingason and Li [22] found that fire spread to a neighbouring wood crib occurs when the ceiling gas temperature above the wood crib rises to about 600 ºC. However, the materials are also a key parameter in fire spread and different materials perform very differently while exposed to the flame radiation. Therefore, the mechanism needs to be known more clearly and also more tests data with different materials are required.

3 Scaling theory

The Froude scaling technique has been applied in this project. It is in most cases not necessary to preserve all the terms obtained by scaling theory simultaneously and only the terms that are most important and most related to the study are preserved. The thermal inertia of the involved material, turbulence intensity and radiation are not explicitly scaled, and the uncertainty due to the scaling is difficult to estimate. However, the Froude scaling has been used widely in enclosure fires. The authors' experience of model tunnel fire tests shows there is a good agreement between model scale and large scale test results [7-9, 24, 25].

The model tunnel was built in a scale of 1:10, which means that the size of the tunnel is scaled geometrically according to this ratio. The scaling of other variables such as the heat release rate, flow rates and the water flow rate can be seen in Table 1. General information about the Froude scaling can be found in the literature [26].

Table 1 A list of scaling correlations for the model tunnel.

Type of unit	Scaling correlations*	Equation number
Heat Release Rate (HRR) $\dot{Q}$ (kW)	$\frac{\dot{Q}_F}{\dot{Q}_M} = (\frac{L_F}{L_M})^{5/2}$	Eq. (1)
Volume flow $\dot{V}$ (m^3/s)	$\frac{\dot{V}_F}{\dot{V}_M} = (\frac{L_F}{L_M})^{5/2}$	Eq. (2)
Velocity u (m/s)	$\frac{u_F}{u_M} = (\frac{L_F}{L_M})^{1/2}$	Eq. (3)
Time t (s)	$\frac{t_F}{t_M} = (\frac{L_F}{L_M})^{1/2}$	Eq. (4)
Energy E (kJ)	$\frac{E_F}{E_M} = (\frac{L_F}{L_M})^{3}$	Eq. (5)
Mass m (kg)	$\frac{m_F}{m_M} = (\frac{L_F}{L_M})^{3}$	Eq. (6)
Temperature T (K)	$T_F = T_M$	Eq. (7)
Pressure difference p (Pa)	$\frac{p_F}{p_M} = \frac{L_F}{L_M}$	Eq. (8)

*Assume the ratio of heat of combustion $\Delta H_{c,M} = \Delta H_{c,F}$. L is the length scale (m). Index M is related to the model scale and index F to full scale (L_M=1 and L_F=10 in our case).

4 Experimental setup

A total of 43 tests were carried out in two model tunnels to investigate the ceiling jet characteristics in SP's large fire hall. The scaling ratio is 1:10, that is, the geometry ratio between model scale and full scale tunnel is 1:10.

4.1 Model tunnel

The model tunnels are 12.5 m long (14.5 m if the fan section is included). The tunnel height is 0.6 m. The tunnel widths are 1 m and 0.6 m. Photos of the tunnels are given in Figure 5 and Figure 6. A schematic drawing of the model tunnel shown in Figure 7.

The model tunnel is constructed using 4 cm thick Promatect L, with the exception of the lower part (50 %) of one side of the tunnel which is covered with a fire resistant window glaze, mounted in steel frames. The Promatect L has a conductivity of 0.083 W/m·K, density of 450 kg/m^3 and heat capacity of 1130 J/kg·K. The material is chosen according to the scaling theory proposed by Li and Hertzberg [25], to simulate concrete and rock used in tunnels (or a mixture of dense and medium dense concrete).

A 1.2 m long tunnel section with grids was used as static box to smooth the flows. The end of the tunnel was set below a smoke hood through which the smoke was exhausted to the central exhaust cleaning system.

Figure 5 Photos of model tunnel A in scale 1:10.

Figure 6 A photo of model tunnel B in scale 1:10.

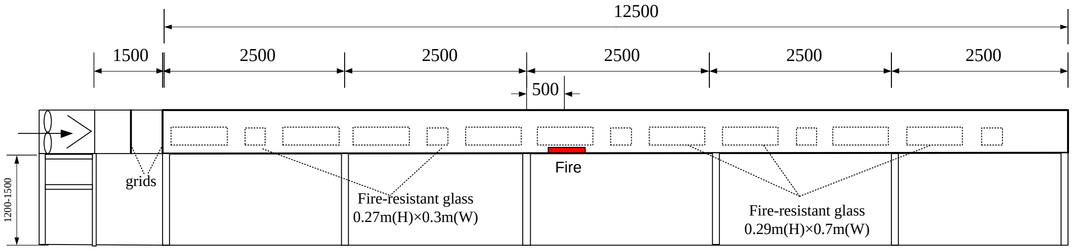

Figure 7 A schematic drawing of the model tunnel (Dimensions in mm).

4.2 Fire source

Gas burners were used as fire sources in the tests in order to easily control the fire. The fire sources were placed in the centre of the model tunnels.

The heat release rates tested are 16 kW, 32 kW, 63 kW, 158 kW, 237 kW, 300 kW, 395 kW,474 kW and 632 kW, corresponding to around 5 MW, 10 MW, 20 MW, 50 MW, 75 MW, 95 MW, 125 MW, 150 MW and 200 MW respectively.

The burner has a cross section of 0.25 m (width) × 0.6 m (length). The height of the burner surface varied among 0, 0.1, 0.2 and 0.3, during the tests. The corresponding fire could be a car fire, a bus fire, or a HGV fire.

4.3 Ventilation system

An axial fan is attached to the end of the tunnel to produce a longitudinal flow in tests with longitudinal ventilation. For the tests with natural ventilation, the fan was removed.

The ventilation velocity varies in a range of 0 m/s to about 2 m/s in model scale, corresponding to 0 to 6.3 m/s in full scale. In one test 3 m/s was used, which corresponds to 9.5 m/s in full scale.

4.4 Fire spread

To investigate the fire spread to neighbouring objects or vehicles, wood and plastic bricks (high Density polyethylene - HDPE) were placed in the tunnel on the floor (7 couples) or 0.2 m above the floor (1 couple) with a free distance of about 1 m in order to model the vehicles, as shown in Figure 8 and Figure 9. One thermocouple and one heat flux meter were placed the targets on the floor. Based on observation of the tests, whether fire spread to these bricks can be determined. This information will be summarized and applied to determine the critical condition for fire spread.

The targets were squares with side length of 5 mm, and thickness of 5 mm and 3 mm for wood and plastic targets respectively. Most of them stayed on the floor but two of them were raised to 0.2 m above the tunnel floor. These targets were changed after every test.
For observation of the flame length during the tests, a ruler (marks) with a resolution of 0.1 m is made along the tunnel.

In tests with the wide tunnel, the plate thermometers were placed beside the center line with one edge attached to the thermocouple tree. Before Test 205, the plastic targets were placed near the windows, at 15 cm from the center line of the tunnel and the wood targets were placed 5 cm from the center line. After Test 205 the locations of the plastic targets were switched with the wood targets.

In the tests with the smaller tunnel, the wood targets were placed closer to the center line of the tunnel, i.e. 6 cm from the center line.

The two targets above floor at Pile D (see Figure 9) were placed 15 cm right behind the targets on the floor.

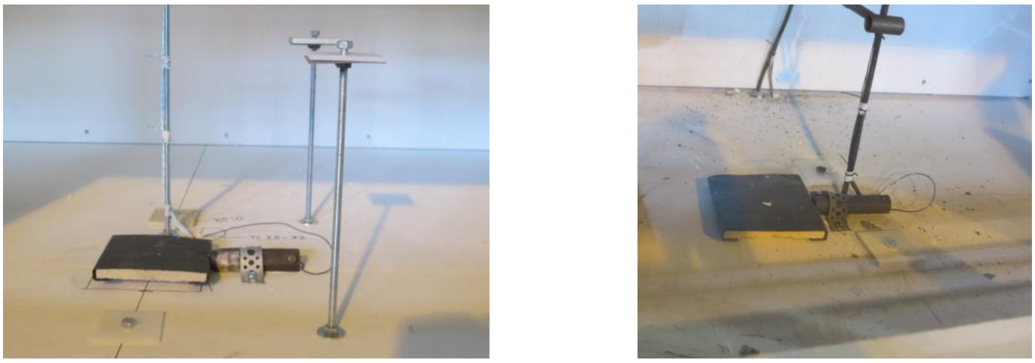

(a) Tunnel A, W=1 m　　　(b) Tunnel B, W=0.6 m

Figure 8　Placement of wood and PE targets in the tunnels

4.5 Measurement

A large amount of thermocouples, bi-directional tubes and plate thermometers, and gas analysis are equipped in model tunnels to measure the characteristics of the ceiling jets in the model tunnels, see Figure 9.

A total of 22 bi-directional tubes will be placed in the vicinity of the fire source, together with thermocouple trees. By combining the measured velocities and the gas temperatures we can obtain the mass flow and heat flow at the cross-sections. Gas analysis were placed at 6 different places. A total of 78 thermocouples were used in the tests, i.e. 8 thermocouple trees with each having 8 thermocouples are placed in the center line of the tunnel at different longitudinal locations and 2 thermocouples trees with each having 4 thermocouples are placed beside two 8-point thermocouple trees. Plate thermometers were placed at 7 locations at the floor close to the small targets and one plate thermometer at the ceiling. Smoke yield was measured using the optical equipment inside the hood system.

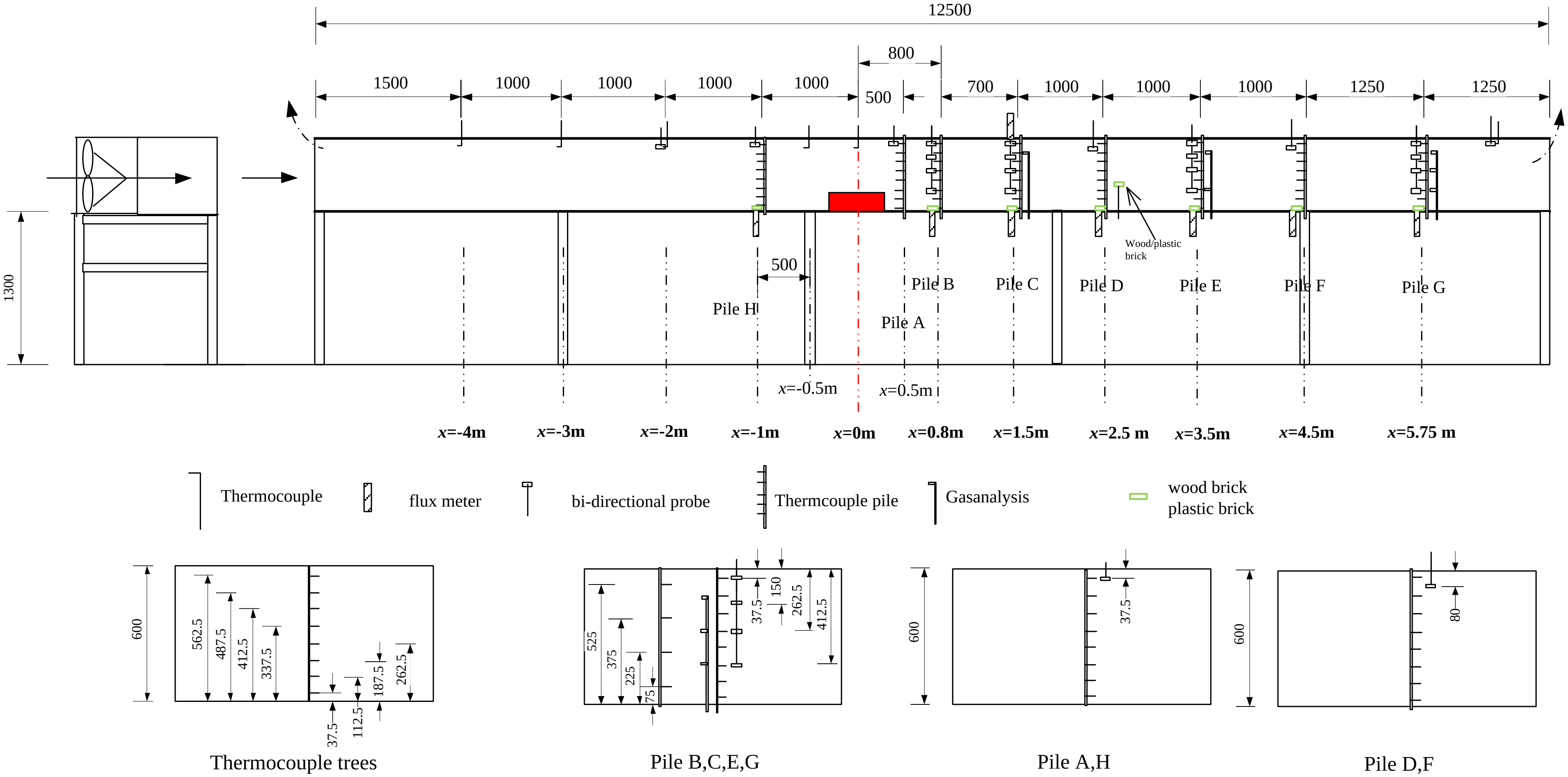

Figure 9 Measurements in the tests (dimensions in mm).

4.6 Estimation of smoke layer interface and mass flow rate

The smoke layer interface is determined from the vertical temperature measurement, by the following equation [27, 28]:

$$h = H - \frac{(I_1 I_2 - H^2)T_1}{I_1 + I_2 T_1^2 - 2HT_1} \tag{9}$$

where

$$I_1 = \int_0^H T(z)dz, \quad I_2 = \int_0^H \frac{1}{T(z)}dz$$

where h is the smoke layer thickness (m), H is tunnel height (m), T_1 is the temperature in the lowest layer [28].

To estimate the smoke flow rates from the tests, a tunnel cross-section is discretized into several layers to calculate the integrals in the above equations. The smoke mass flow rate, $\dot{m}$ (kg/s), is estimated by:

$$\dot{m} = \xi \int_{H-h}^{H} \rho(z)u(z)Wdz, \tag{10}$$

where ξ is flow coefficient and W is tunnel width. In the calculations, a theoretical value of ξ =0.817 was used [29]. ρ is gas density (kg/m^3), u is gas velocity (m/s), and z is height above floor (m).

Note that it is assumed that the properties of the smoke flow across one horizontal tunnel cross-section is uniform within the smoke layer. Further, in tests with longitudinal ventilation, the fire plume is deflected and the ceiling impingement point of the fire plume varies with ventilation velocity, however the measurement points were fixed in the tests. In order to estimate the initial ceiling jet flow rate, the measurement point downstream of the impingement point is considered as the initial location for the ceiling jet. These two assumptions may result in slight overestimation of the initial ceiling jet flow rate. Therefore the estimated initial ceiling jet flow rates are regarded as conservative.

5 Test procedure

A summary of tests carried out in this project is listed in Table 2. W is tunnel widthNote that the corresponding full scale values for $\dot{Q}$ can easily be obtained by Eq. (1).

The measurements were started 2 min before ignition. In each test, either the ventilation velocity is fixed with a varying heat release rate, or the heat release rate is fixed with a varying velocity. For example in test 101, the velocity is fixed at 2 m/s while the heat release rate is varied. After ignition at 2 min, the heat release rate was 16 kW for 8 min, and then changed to 32 kW for 5 min, to 63 for 5 min, to 158 for 5 min, to 300 kW for another 5 min and then extinguished.

In tests 107, 108 and 603, the fan was detached from the main tunnel and placed 1.5 m from the portal. The velocities correspond to the initial air velocity inside the tunnel and may vary slightly during the tests.

Two cameras were used to film the tests with one placed at the exit of the tunnel and one on one side of the tunnel. These films were used to analyse the smoke distribution and ignition time of the targets.

Table 2 Summary of tunnel fire tests.

Test no.	W	h_b	u_o	$\dot{Q}$	Duration**
8 tests	m	m	m/s	kW	min
101	1	0.1	2	16,32,63,158,300	30 min (2+8+5+5+5+5 min)
102	1	0.1	1.5	16,32,63,158,300	30 min (2+8+5+5+5+5 min)
103	1	0.1	1	16,32,63,158,300	30 min (2+8+5+5+5+5 min)
104	1	0.1	0.5	16,32,63,158,300	30 min (2+8+5+5+5+5 min)
105	1	0.1	2-1-0.5	474	15 min (2+5+5+3min)
106	1	0.1	2-1	632	10 min (2+5+3min)
107*	1	0.1	0.5	16,32,63,158,300,474	31 min (2+8+5+5+5+3+3 min)
108*	1	0.1	1	16,32,63,158,300,474,632	34 min (2+8+5+5+5+3+3 min)
201	1	0.3	2	16,32,63,158,300	30min (2+8+5+5+5+5 min)
202	1	0.3	1.5	16,32,63,158,300	30min (2+8+5+5+5+5 min)
203	1	0.3	1	16,32,63,158,300	30min (2+8+5+5+5+5 min)
204	1	0.3	0.5	16,32,63,158,300	30min (2+8+5+5+5+5 min)
205	1	0.3	2-1-0.5	474	17min (2+5+5+5min)
207	1	0.3	0.75	16,32,63,158,300	30min (2+8+5+5+5+5 min)
301	1	0.2	2	16,32,63,158,300	30min (2+8+5+5+5+5 min)
302	1	0.2	1	16,32,63,158,300	30min (2+8+5+5+5+5 min)
303	1	0.2	2-1-0.5	150	15min (2+5+5+3 min)
401	1	0	2	16,32,63,158,300	30min (2+8+5+5+5+5 min)
402	1	0	1	16,32,63,158,300	30min (2+8+5+5+5+5 min)
403	1	0	2-1	150	15min(2+5+5+3 min)
405	1	0	0.85	16,32,63,158,300	30min (2+8+5+5+5+5 min)
501	1	0.1	0	16,32,63,158,300,474,632	31min(2+5+5+5+5+3+3+3min)
502	1	0.3	0	16,32,63,158,300,474	28min (2+5+5+5+5+3+3min)
601	0.6	0.1	0	16,32,63,158,237,300,395	29min(2+5+5+5+3+3+3+3min)
602	0.6	0.3	0	16,32,63,158,237,300,395	27.5min(2+5+5+5+3+3+3+1.5min)
603	0.6	0.1	1.6-0.8-0.5-0.3	300	13min (2+3+3+3+2min)
701	0.6	0.1	2	16,32,63,158,237,300,395	29min(2+5+5+5+3+3+3+3min)
702	0.6	0.1	1.5	16,32,63,158,237,300,395	29min(2+5+5+5+3+3+3+3min)
703	0.6	0.1	1	16,32,63,158,237,300,395	29min 2+5+5+5+3+3+3+3min)

704	0.6	0.1	0.75	16,32,63,158,237,300,395	29min(2+5+5+5+3+3+3+3min)
705	0.6	0.1	0.5	16,32,63,158,237,300,395	29min(2+5+5+5+3+3+3+3min)
801	0.6	0.3	2	16,32,63,158,237,300,395	29min(2+5+5+5+3+3+3+3min)
802	0.6	0.3	1.5	16,32,63,158,237,300,395	29min(2+5+5+5+3+3+3+3min)
803	0.6	0.3	1	16,32,63,158,237,300,395	29min(2+5+5+5+3+3+3+3min)
804	0.6	0.3	0.75	16,32,63,158,237,300,395	29min(2+5+5+5+3+3+3+3min)
805	0.6	0.3	0.5	16,32,63,158,237,300,395	29min(2+5+5+5+3+3+3+3min)
901	0.6	0	3	16,32,63,158,237,300,395	29min(2+5+5+5+3+3+3+3min)
902	0.6	0	2	16,32,63,158,237,300,395	29min(2+5+5+5+3+3+3+3min)
903	0.6	0	1	16,32,63,158,237,300,395	29min(2+5+5+5+3+3+3+3min)
904	0.6	0	0.5	16,32,63,158,237,300,395	29min(2+5+5+5+3+3+3+3min)
905	0.6		2-1-0.5	632	10.5 min (2+3+3+2.5min)
1001	0.6	0.2	2	16,32,63,158,237,300,395	29min(2+5+5+5+3+3+3+3min)
1002	0.6	0.2	1	16,32,63,158,237,300,395	29min(2+5+5+5+3+3+3+3min)

*One tunnel end open but blow air using the fan placed 1.5 m away from the portal.
**the parameter changes gradually at the corresponding time.

6 Results and discussion

Test results are analyzed based on the theoretical approach presented in the appendixes. It include a specific focus on the initial one-dimensional conditions for the fire-induced ceiling jets in tunnels under different ventilation conditions.

6.1 Flame length

According to the theoretical model in Appendix A, the ceiling flame length is proportional to heat release rate and inversely proportional to the tunnel width. Further, the effective tunnel height is also a key parameter for the flame length in tunnel fires.

Under low ventilation rate conditions, two parts of the flame exist: upstream and downstream of the fire, respectively, while the ceiling flames only exist downstream of the fire under high ventilation conditions.

In the tests, it was observed that under high ventilation, the continuous flame region and the intermittent flame region [30] can be identified, similar to that for the fire plumes in the open. In other words, the flames close to the flame tips were detached under such conditions. The continuous flame lengths are approximately 75 % to 85 % of the flame lengths defined based on the flame tips.

There is a special case in the performed test series that needs special attention. In some tests with a velocity of around 0.5 m/s (or even slightly higher), the upstream flame descended to the floor level. Note that under such conditions, significant backlayering existed, and length of the reverse flows could be much longer than the upstream tunnel section length. However, the reverse flows after reaching the upstream end cannot spread any further due to the end of the tunnel. Note that the end of the tunnel was attached to a filter and a fan that was designed to prevent any smoke spreading into it (at least in most of the tests). This resulted in a reverse flows that were blown back towards the fire. The air flows from the filter with a much higher velocity due to the disturbed flow patterns and consequently the reversed air flows were highly vitiated, which were known from the smoke layer height upstream of the fire. In reality, if the tunnel is short, this part of reverse flow could flow out of the tunnel (as the cases with natural ventilation), or if the tunnel is very long, the reverse flow could travel to a position far from the fire and take a long time to return back to the fire site. In both cases, stratification of the backlayering should be much better than the special case in the tests. In other words, in some tests with low velocities, the fresh air flow were highly vitiated, and the fires were even locally under-ventilated in the vicinity of the fire site. From the theoretical model, the vitiated air results in a lower oxygen concentration of the inflow, Y_{O2}. This indicates that the flame length can be slightly longer. Under such low ventilation conditions, there is no clear distinction between continuous flame and intermittent flame, and the flame appears to be continuous although the combustion is still unstable.

In the following, the flame lengths discussed, L_f, are defined as the distance between the flame tip and the center of the fire source, as shown in Figure 3 and Figure 4. For fires with flames not reaching the ceiling, the horizontal lengths of the inclined flames are estimated and used as the downstream flame lengths.

6.1.1 Downstream flame lengths

The downstream flame lengths measured in test series 7 (test 701 to test 705) and test 601 are shown in Figure 10. Clearly, for a given velocity, a linear correlation between the downstream flame length and the heat release rate can be found. The flame lengths were determined by visual observations during the tests.

Further, it can be found from Figure 10 that for a given heat release rate, the downstream flame lengths with different velocities are approximately the same. This indicates that the influence of the ventilation velocity on the downstream flame lengths is limited. The largest difference in the downstream flame lengths between two points with different velocities is around 16 %. It can also be found that for a given heat release rate higher than 100 kW, the downstream flame lengths reaches maximum values when the velocities are between 0 m/s and 1 m/s, i.e. around 0.5 m/s. This can be explained by the highly vitiated inflows, as described previously.

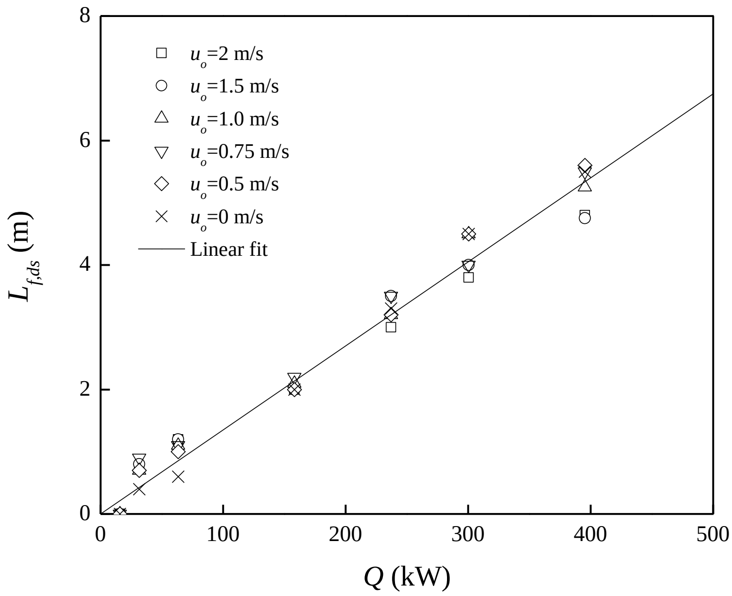

Figure 10 Downstream flame lengths in test series 7 and test 601.

To normalize the results, two dimensionless parameters are defined here. The dimensionless flame length is defined as:

$$L_f^* = \frac{L_f}{H} \tag{11}$$

The dimensionless heat release rate is defined as:

$$\dot{Q}_f^* = \frac{\dot{Q}}{\rho_o c_p T_o g^{1/2} A H_{ef}^{1/2}} \tag{12}$$

where c_p is heat capacity (kJ/kgK), A is tunnel cross-sectional area (m^2), H_{ef} is effective tunnel height (vertical distance between fire source bottom and tunnel ceiling) (m), H is tunnel height(m), $\dot{Q}$ is heat release rate (kW), ρ_o is ambient air density (kg/m^3), T_o is ambient air temperature (K), g is gravity acceleration (m/s^2).

According to the theoretical analysis in Appendix A, it is known that the dimensionless flame length is proportional to the dimensionless heat release rate:

$$L^*_{f,ds} = C_f Q^*_f \qquad (13)$$

where C_f is a coefficient which will be determined by experimental data and subscript *ds* indicates downstream. It can be seen that the flame length is independent of the ventilation velocity, under the above assumptions. The downstream flame length is mainly a function of heat release rate, tunnel width and effective tunnel height.

Figure 11 shows all the test data for the dimensionless downstream ceiling flame length. The test data include the tests with natural ventilation and high ventilation.

It is shown in Figure 11 that all the test data even those with natural ventilation can be correlated well with the proposed equation. This also indicates that under natural ventilation, the total flame length will be longer and can be as long as twice the downstream flame length. This could be due to the limited mixing in cases with natural ventilation. It is known that the combustion is mixing controlled in most practical tunnel fires, which indicates the chemical reaction time is infinitesimal compared to the mixing time. In contrast, in cases with longitudinal ventilation, the mixing is much better.

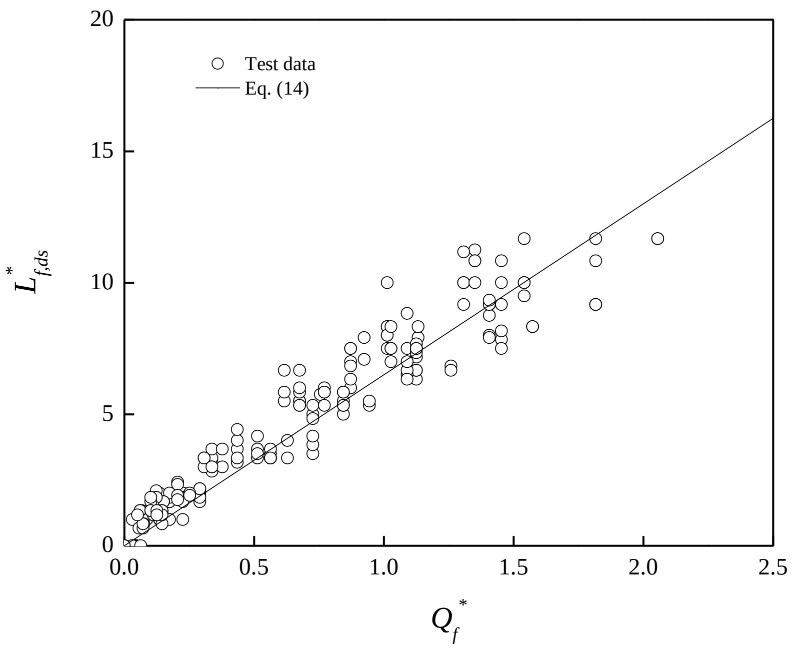

Figure 11 Correlation for the downstream flame length for all the tests.

Figure 12 shows the dimensionless flame lengths under high ventilation as a function of the dimensionless heat release rate, including data from longitudinal tunnel fire tests conducted at SP [16], point extraction tests also conducted at SP [22], EUREKA 499 programme [12], Memorial tunnel tests [13] and Runehamar tests [31].

It can be concluded that under high ventilation, the flame length in a tunnel fire is mainly dependent on the heat release rate, tunnel width and the effective tunnel height, and insensitive to the ventilation velocity. Clearly, the proposed equation correlates well with the test data. The correlation can be expressed as:

$$L^*_{f,ds} = 6.0 Q^*_f \tag{14}$$

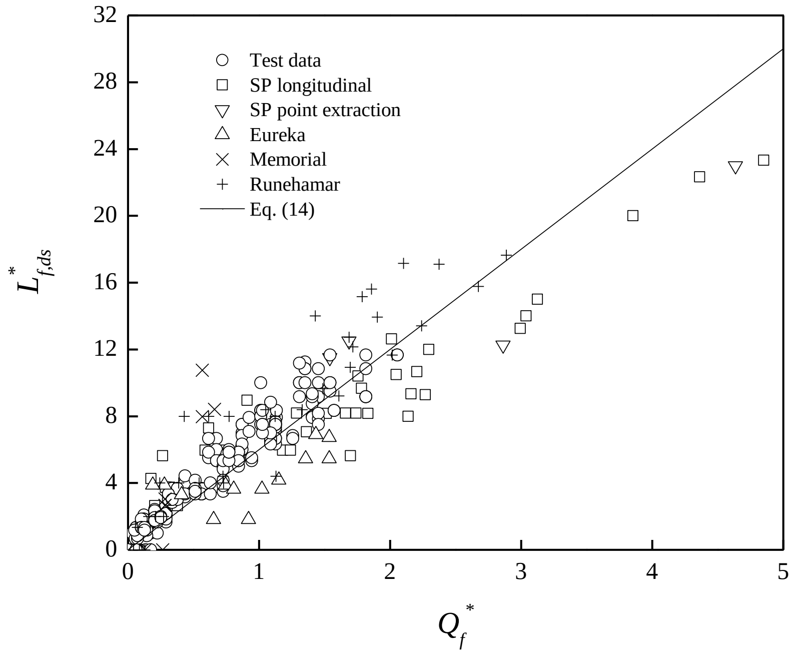

Figure 12 Correlation for the dimensionless downstream flame length.

6.1.2 Upstream flame lengths

If the longitudinal ventilation velocity is much lower than the critical velocity, i.e. the minimum longitudinal ventilation velocity to prevent any smoke reverse flow, there exist two parts of horizontal flames, i.e. downstream flame ($L_{f,ds}$) and upstream flame ($L_{f,us}$). For high ventilation velocities, only the downstream flames exist. The transition point is therefore defined as the minimum longitudinal velocity above which no ceiling flame exists upstream of the fire source. Accordingly, the “high ventilation” for the flame length is defined as the case with the ventilation velocity larger than the transition point, and the “low ventilation” corresponds to the ventilation velocity less than the transition point.

According to Li et al.’s work [7], the ratio of backlayering length to the tunnel height is related to the ratio of the ventilation velocity to the critical velocity at a given heat release rate. For high heat release rates, the backlayering length is only dependent on the ventilation velocity, regardless of the heat release rate. Note that the upstream flame length is part of the backlayering length, and the fires with ceiling flames only correspond to high heat release rates. Therefore, similar to the critical velocity, a dimensionless ventilation velocity at the transition point is defined:

$$u^*_{tp} = \frac{u_{o,tp}}{\sqrt{gH}} \tag{15}$$

Another dimensionless heat release rate was defined according to the following equation:

$$Q^* = \frac{\dot{Q}}{\rho_o c_p T_o g^{1/2} H^{5/2}} \tag{16}$$

where u_o is the longitudinal velocity (m/s). Subscript *tp* indicates transition point.

Figure 13 shows a plot of data with and without upstream flames. The solid data points represent a situation when the flames existed on the upstream side in the tests, and the hollow data points indicate when no flames were obtained on the upstream side for different longitudinal velocities. The data show that there is a clear transition line that exists between the solid and hollow data points. This line can be expressed as:

$$u_{tp}^* = 0.3 \tag{17}$$

Given that the dimensionless critical velocity approaches 0.43 for large fires [7], the results shown in Figure 13 indicate that the transition point corresponds to a longitudinal velocity of approximately 70 % of the critical velocity, and the corresponding dimensionless backlayering length is around 7 [7].

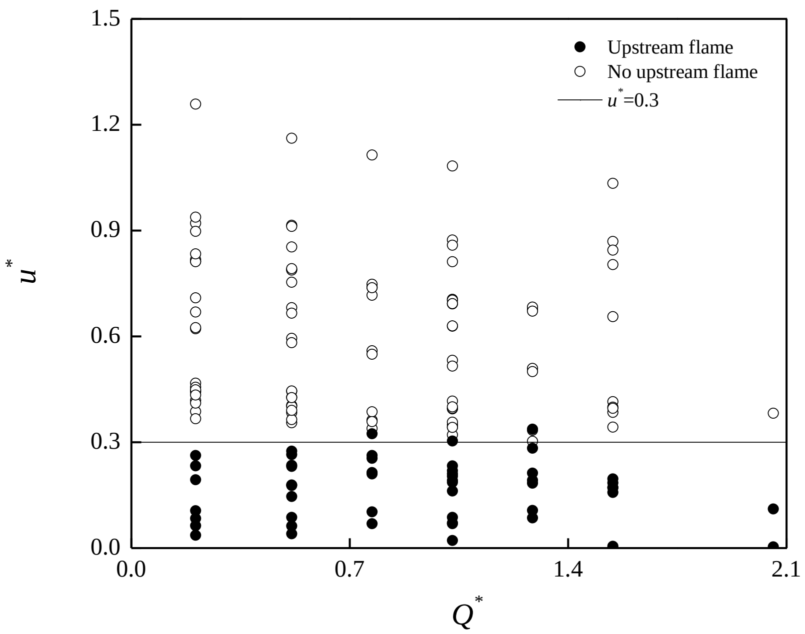

Figure 13. Transition line between low and high ventilation rate for all the tests.

Large scale test data are also used for further verification of this transition point. Figure 14 show a plot of data with and without upstream flames from longitudinal tunnel fire tests conducted at SP [16], point extraction tests also conducted at SP [22], the Memorial tunnel tests [13] and the Runehamar tests [31] are used in the analysis. The transition point also corresponds to a dimensionless velocity of 0.3.

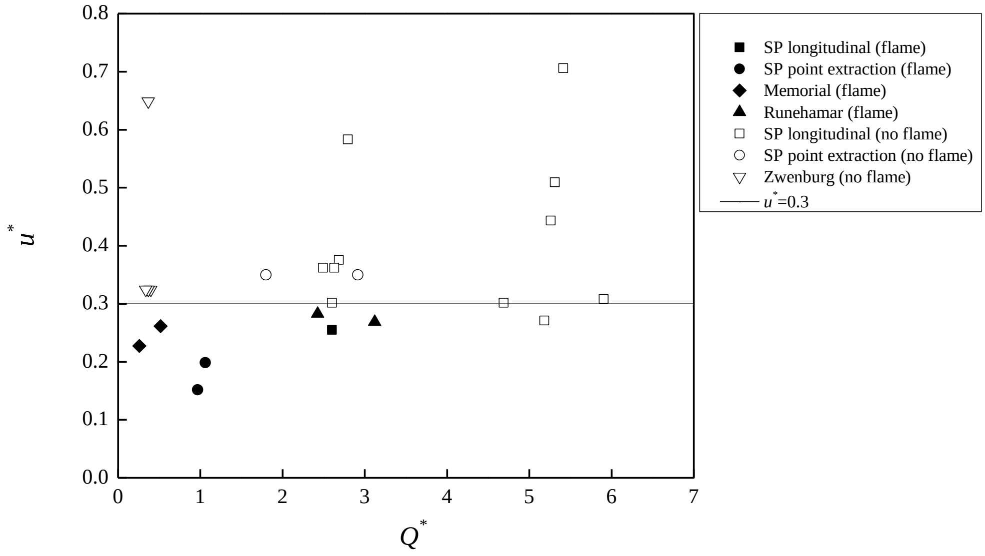

Figure 14 Transition point between low and high ventilation rate for some full scale tests and other model scale tests.

It should be noted that the upstream flame length will not exist in case that the heat release rate is too low to allow the flame touches the ceiling even if the velocity fulfils this criteria.

There is a need to know how the upstream flame length varies with the longitudinal ventilation velocity, compared to the downstream flame length.

Figure 15 shows the ratio of upstream flame length to downstream flame length as a function of the dimensionless ventilation velocity. Clearly, increasing velocity results in a decreased ratio between upstream and downstream flame lengths. The proposed equation can be expressed as:

$$L_{f,\mathrm{us}} = C_u L_{f,\mathrm{ds}} \quad \text{or} \quad L^*_{f,\mathrm{us}} = C_u L^*_{f,\mathrm{ds}} \tag{18}$$

where the correction factor, C_u, :

$$C_u = \begin{cases} 1 - 3.3u^* & u^* < 0.3 \\ 0 & u^* \geq 0.3 \end{cases}$$

Note that if u^*>0.3, there is no upstream flame and thus the value of C_u=0.

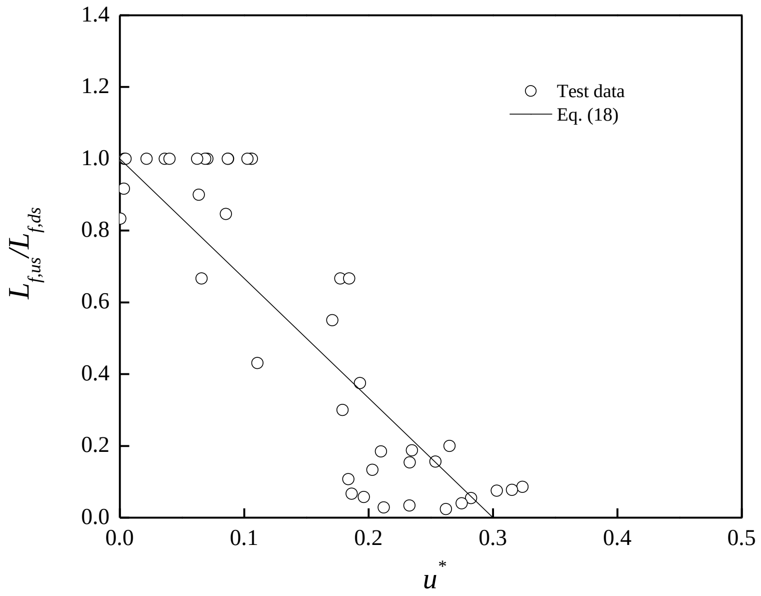

Figure 15 Upstream flame length under low ventilation rate.

6.1.3 Total flame length

The dimensionless total flame length can be estimated by:

$$L^*_{f,tot} = L^*_{f,\mathrm{us}} + L^*_{f,\mathrm{ds}} = (1 + C_u)L^*_{f,\mathrm{ds}} = 6(1 + C_u)Q^*_f \tag{19}$$

Thus, as the ventilation velocity decreases, the total flame length increases as seen in Eq. 18, although the downstream flame length is approximately invariant. In other words, the increase of total flame length due to a lower ventilation velocity is due to the existence of the upstream flame.

A special case is the fire *under low ventilation rate* (velocity close to zero, no dominating flow direction, C_u=1), where the total flame length can be simply expressed as:

$$L^*_{f,tot} = 2L^*_{f,\mathrm{ds}} = 12Q^*_f \tag{20}$$

Figure 16 shows the dimensionless total flame lengths under low ventilation conditions as a function of the dimensionless heat release rate. Test data from EUREKA 499 programme [12], Memorial tunnel tests [13] and Hinkley's tests [32] were used. Note that in Hinkley's tests [32] the fire sources were attached to one closed end, and thus the scenario could be considered as being symmetrical, i.e. both the flame lengths and heat release rates are doubled while plotting in the figure. It is clearly shown that the proposed equation correlate very well with the test data.

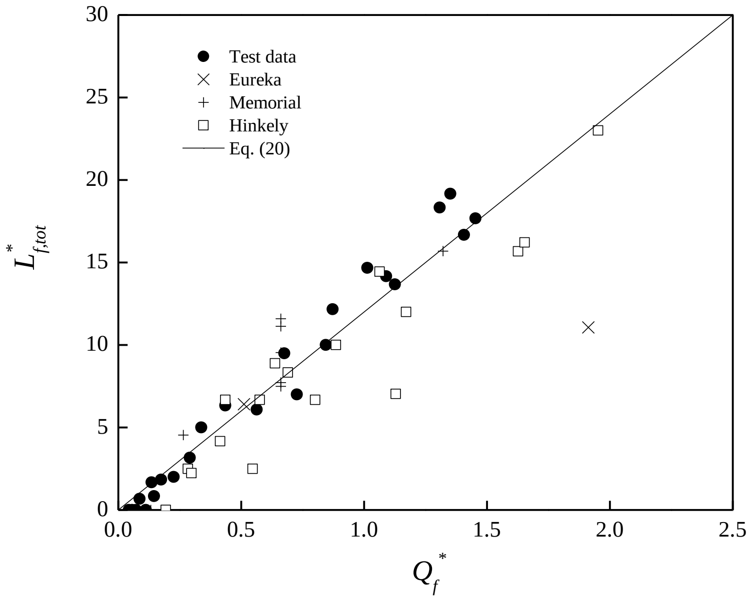

Figure 16 Total flame length under low ventilation rate.

6.2 Ceiling jet velocity

A theoretical model of initial smoke velocity of the ceiling jet in a tunnel fire is presented in Appendix B.

6.2.1 Low ventilation or natural ventilation

According to the theoretical analysis in Appendix B, the gas velocity for the initial ceiling jet under natural ventilation can be expressed as follows:

$$u_g = C(\frac{H_{ef}}{W})^{1/2}(\frac{\dot{Q}}{H_{ef}})^{1/3} \quad (21)$$

where *C* is a correction factor. The above equation indicates that the main parameters for initial ceiling jet velocities under natural ventilation are the heat release rate and tunnel geometry.

Figure 17 shows the initial ceiling jet gas velocities in tests with natural ventilation. It can be seen that all the data correlate well with the following correlation:

$$u_g = 0.3(\frac{H_{ef}}{W})^{1/2}(\frac{\dot{Q}}{H_{ef}})^{1/3} \quad (22)$$

The slope of the regression line in Figure 17 follows *C*=0.3.

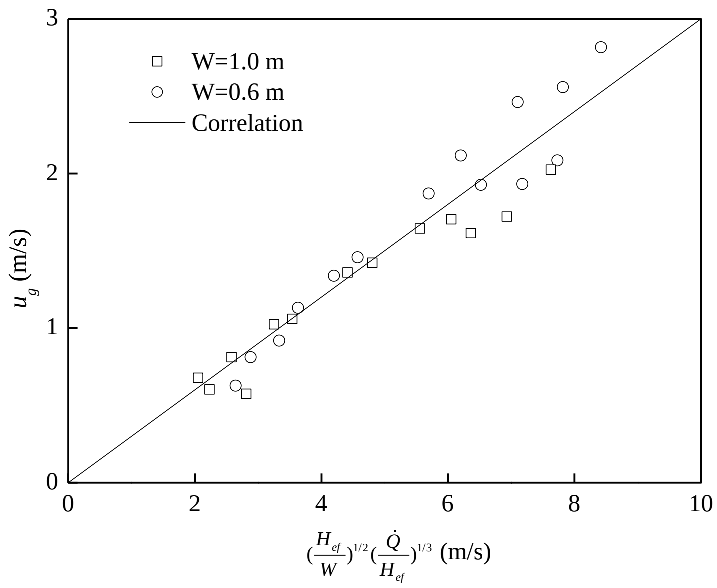

Figure 17 Ceiling jet velocity under natural ventilation.

6.2.2 High ventilation

According to the theoretical analysis in Appendix B, the gas velocity for the initial ceiling jet under high ventilation can be expressed as follows:

$$u_g = u_o \sqrt{1 + \frac{\Delta T_{\max}}{T_o}} \tag{23}$$

where $\Delta T_{\max}$ is the maximum ceiling excess gas temperature, which can be estimated using the equation proposed by Li et al. [8-10], i.e. Equation (33) in Section 6.4. The influencing parameters include heat release rate, velocity, location height, and tunnel width.

Data from test series 7 are plotted firstly to check the reasonability of the equation, see Figure 18. Clearly, the estimated gas velocities according to Eq. (23) correlate very well with the measured gas velocities for test series 7.

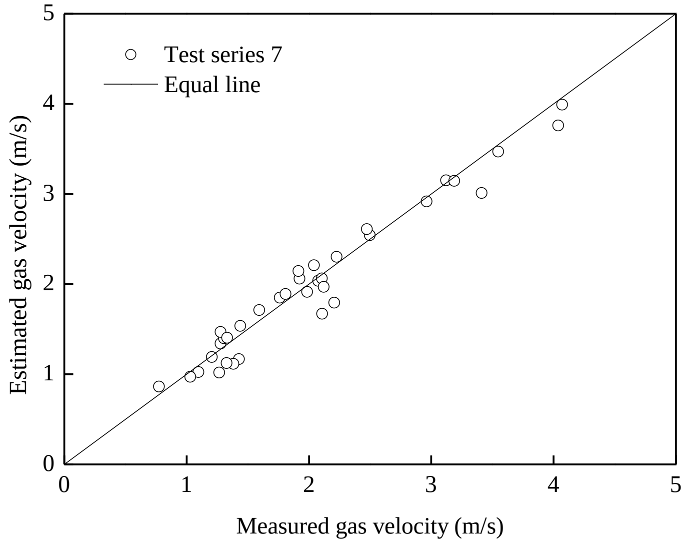

Figure 18 Comparison of ceiling jet velocities estimated by Eq. (23) and measured values under high ventilation for test series 7.

Figure 19 shows the comparison of measured gas velocities under high ventilation and the estimated values. Clearly, most data lie close to the equivalent line. This indicates that Equation (23) can well predict the gas velocity of the ceiling jet in tunnels under high ventilation.

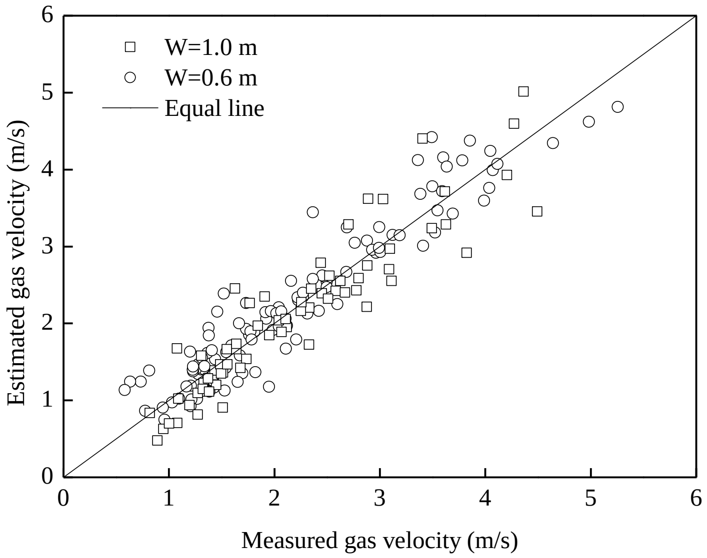

Figure 19 Comparison of ceiling jet velocities estimated by Eq. (23) and measured values for all the tests.

6.3 Ceiling jet flow rate

The previous work [8] obtained correlations for the mass flow rate of a ventilated fire plume at different height. By ignoring the entrainment in the impingement region, the mass flow rate of the initial ceiling jet at the ceiling level could be expressed as:

$$\dot{m}_p(z) = \begin{cases} 0.071\dot{Q}_c^{1/3} H_{ef}^{5/3}, & V' \le 0.19 \\ 0.3735\dot{Q}_c^{1/3} H_{ef}^{5/3} V', & V' > 0.19 \end{cases} \quad (24)$$

This above equation can also be expressed as:

$$\dot{m}_p(z) = \begin{cases} 0.071\dot{Q}_c^{1/3} H_{ef}^{5/3}, & V' \le 0.19 \\ 1.1 u_o H_{ef}^{5/3} b_{fo}^{1/3}, & V' > 0.19 \end{cases} \quad (25)$$

where the dimensionless ventilation velocity, V', is defined as:

$$V' = u_o / (\frac{g\dot{Q}}{b_{fo}\rho_o c_p T_o})^{1/3} \quad (26)$$

where $\dot{Q}_c$ is convective heat release rate, H_{ef} is effective tunnel height, b_{fo} is radius of fire source (m). The equation indicates that for a low velocity, the mass flow rate of the fire plume is independent of velocity and increases with heat release rate and effective tunnel height. For a high velocity, the smoke mass flow rate increases linearly with ventilation velocity, independent of heat release rate.

Generally, the entrainment in the impingement region is not negligible. Strong vortexes in this region were observed in the tests. However, it could be reasonably assumed that the formulation of the equations still work for the initial ceiling jet flow rate.

6.3.1 Low ventilation or natural ventilation

Here the natural ventilation (tunnel open in both ends) means a quiescent environment in the tunnel, that is, the scenario is assumed to be symmetrical. In many cases, a fire in a tunnel with natural ventilation may also produce a longitudinal flow with a significantly large velocity, especially for a fire in a tunnel section with a large slope. This, however, can be classified as high ventilation.

Figure 20 shows the mass flow rate of the initial ceiling jet in tunnels under natural ventilation. The following equation can be used:

$$\dot{m}_g = 0.058\dot{Q}^{1/3} H_{ef}^{5/3} \quad (27)$$

Note that the above equation is similar to the equation for mass flow rate of a free plume. However, the heat release rate in the above equation $\dot{Q}$ is the total heat release rate rather than the convective heat release rate as used for free plume. It should be kept in mind that the above equation corresponds to smoke flow rate on one side. This finding does not affect the correlations for maximum gas temperatures as the coefficients of the equations were obtained from test data.

According to the symmetry of the scenarios, the total smoke flow rate from a tunnel fire under natural ventilation should be doubled:

$$\dot{m}_{g,tot} = 0.12\dot{Q}^{1/3} H_{ef}^{5/3} \quad (28)$$

This equation could be used for rough estimation of total mass flow rates from small or large tunnel fires in the vicinity of the fire site.

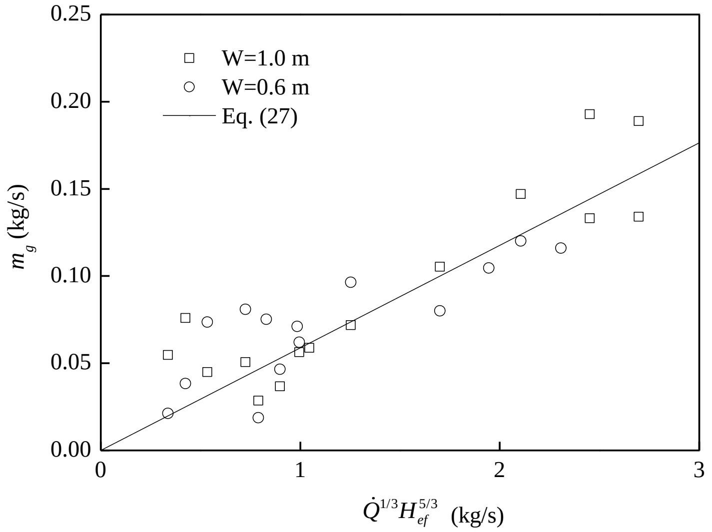

Figure 20 Correlation for the smoke mass flow rate under natural ventilation.

6.3.2 High ventilation

At first a simple parametric study is carried out. Figure 21 shows the smoke mass flow rate as a function of ventilation velocity and heat release rate for Test series 7. Note that for any given heat release rate, the smoke mass flow rate increases linearly with ventilation velocity. Further, there appears to be no difference in the smoke mass flow rate between different heat release rates. This indicates that in tunnel fires under forced ventilation, the effect of the heat release rate on the mass flow rate of the ceiling jet is negligible.

The above analysis fully supports the equation for the mass flow rate.

For velocities close to 0.5 m/s, the measured smoke mass flow rate is slightly lower. This could be mainly due to that under low ventilation backlayering exists, and the vertical fire plume splits into two parts: upstream and downstream. Although in these tests the backlayering was arrested and pushed towards downstream, the temperature of these arrested flow was reduced significantly and thus the method used for determining the smoke layer height could underestimate the smoke layer height somewhat.

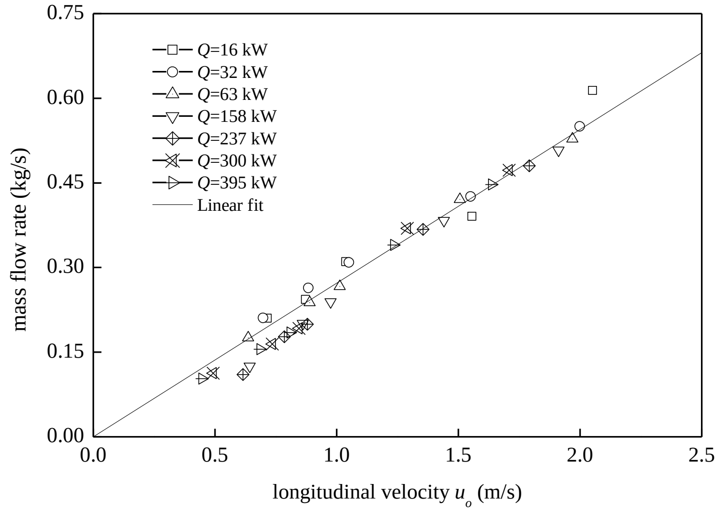

Figure 21 Smoke mass flow rate vs. ventilation velocity and heat release rate for Test series 7.

Figure 22 shows the smoke mass flow rate as a function of ventilation velocity and heat release rate for all the tests with forced ventilation. Apparently the deviation of data from Tunnel A tests is much greater than Tunnel B tests. The reason could be that larger error is introduced while estimating the mass flow rate for the wide tunnel as the properties across some horizontal cross sections are far from uniformity.

The following equation which best fits all the test data for mass flow rate of the initial ceiling jet is proposed:

$$\dot{m}_g = 1.1 u_o H_{ef}^{2/3} b_{fo}^{1/3} W \tag{29}$$

This equation slightly differs from the theoretical equation for initial flow rate of ceiling jets. In reality, the measured mass flow rates correspond to the state after impingement on ceiling and then the tunnel walls. It was observed from the tests that large vortexes were produced while the smoke flow impinged on the two side walls. This process can apparently entrain a large amount of air flows into the smoke volume, and this entrainment rate could be proportional to tunnel width *W*. Further, it should be noticed while estimating the mass flow rates from the test data, it is assumed that the smoke is evenly distributed along the tunnel width. This could somewhat overestimate the mass flow rates, leading to conservative results.

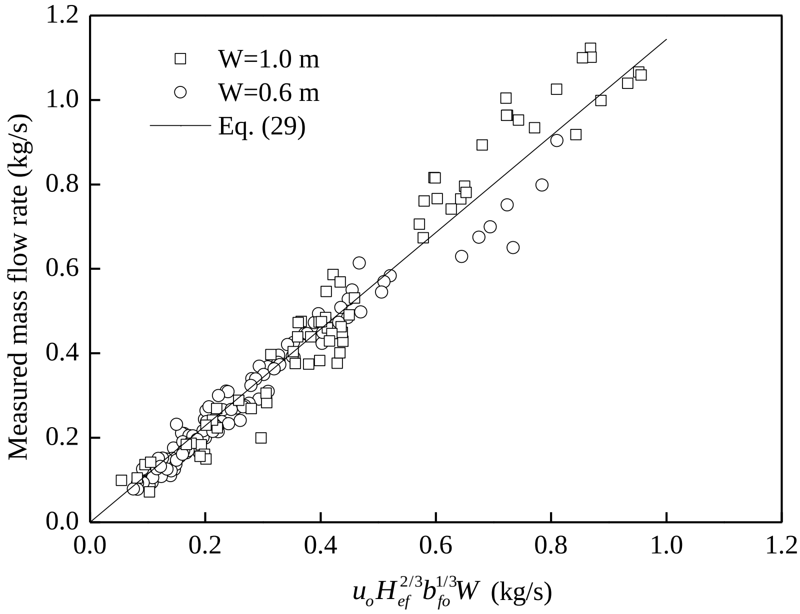

Figure 22 Correlation for the smoke mass flow rate under high ventilation.

6.3.3 Correlation for total smoke flow rate

To simplify the calculation, the greater smoke flow rate estimated using the two methods are the total smoke flow rate, which can be expressed by:

$$\dot{m}_{g,tot} = \max\left(0.12 Q^{1/3} H_{ef}^{5/3}, 1.1 u_o H_{ef}^{2/3} b_{fo}^{1/3} W\right) \tag{30}$$

The first term is greater for low ventilation while the second term will is greater for high ventilation. This simplifies the need to distinguish the low and high ventilation regions.

It should be pointed out that all data for smoke flow rates are estimated assuming that the properties of the smoke flow across one horizontal tunnel cross-section is uniform. Further, the position slightly further away from the impingement point is considered as the initial location for the ceiling jet. These two assumptions may result in slight overestimation of the mass flow rate and therefore conservative results, as pointed out in Section 4.6.

The equation could be used for estimation of total smoke flow rate or smoke release rate from a fire in a tunnel under natural or forced ventilation. Note that in most handbooks and textbooks, the smoke flow rate from a fire is considered as constant for a given heat release rate. However, it has been proven in this work that the mass flow rate strongly depends on the ventilation velocity. Only for a fire in a tunnel with very low velocity across the fire, the smoke flow rate is independent of the ventilation velocity, instead, it is only a function of heat release rate and effective tunnel height.

6.4 Ceiling jet temperature

Ceiling jet temperature is of great importance for assessment of heat exposure to tunnel users and tunnel structures, estimation of fire detection time and possibility of fire spread, and to design ventilation systems.

A theoretical model of distribution of gas temperature of the ceiling jet in a tunnel fire is presented in Appendix C.

Figure 23 shows an example of the centreline temperature contours in test 701 with a velocity of 1 m/s and different heat release rates. Note that the resolution of the temperature is not high enough in the vicinity of the fire source where highest temperature gradients exist. For larger fires, the temperature close to floor could be as high as 500 °C to 600 °C indicating that the flame descended to a position close to the floor. For fires not greater than 20 MW, there appears to be clearer vertical temperature gradient. However, strictly speaking, smoke stratification downstream of the fire does not really exist in the tests with 1 m/s, corresponding to approx. 3 m/s in full scale.

It is observed from the tests that smoke stratification downstream of the fire only exist for fires not greater than 20 MW and very low velocities. In most tests the smoke layer height downstream of the fire is around 0.05 m to 0.1 m above the floor.

Comparisons of observed flame tips and the temperature measurement indicate that the temperature at flame tip is mostly in a range of 500 °C to 650 °C. No single value for temperature at the flame tip can be identified.

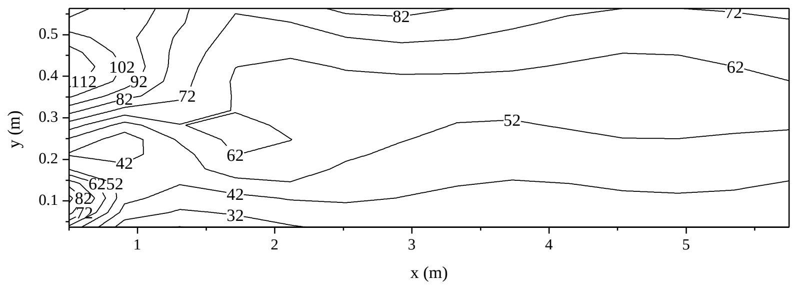

(a) 16 kW (5 MW)

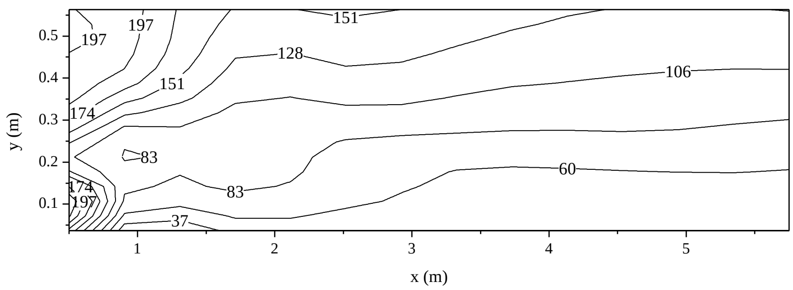

(b) 32 kW (10 MW)

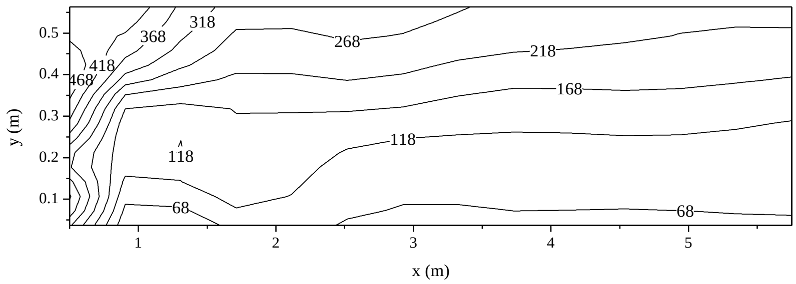

(c) 63 kW (20 MW)

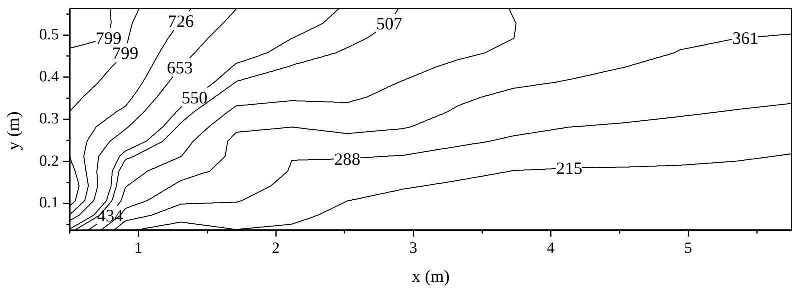

(d) 158 kW (50 MW)

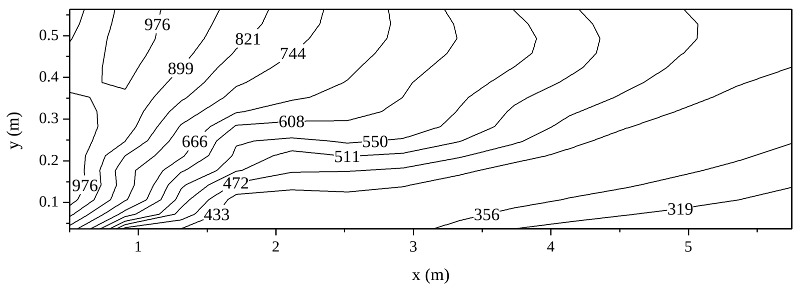

(e) 237 kW (75 MW)

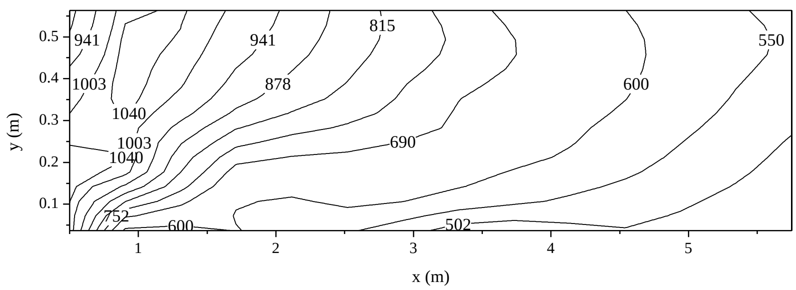

(f) 300 kW (95 MW)

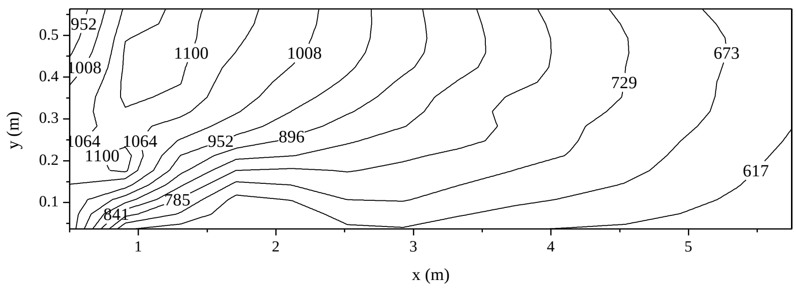

(g) 395 kW (125 MW)

Figure 23 Gas temperature contour along the tunnel centreline in test 703 with a velocity of 1 m/s and different heat release rates. y is the tunnel height and x is the distance from the fire source.

6.4.1 Maximum ceiling temperature

Li et al [8-10] proposed the following equations for maximum ceiling excess gas temperature in tunnel fires under different ventilation conditions. The maximum temperature beneath the ceiling in a tunnel fire is independent of the ventilation velocity if the ventilation velocity across the fire source is very low compared to the heat release rate, and the maximum temperature is simply dependent on the heat release rate; however, it approaches a constant if the part of the flame volume containing the combustion zone is present at the tunnel ceiling. In other words, if $V' \leq 0.19$ (Region I), the maximum excess temperature can be expressed as:

$$\Delta T_{\max} = \begin{cases} \mathrm{DTR\,I}, & \mathrm{DTR\,I} < 1350 \\ 1350, & \mathrm{DTR\,I} \geq 1350 \end{cases} \tag{31}$$

where the Delta T in Region I, DTRI, is defined as:

$$\mathrm{DTR\,I} = 17.5 \frac{\dot{Q}^{2/3}}{H_{ef}^{5/3}}$$

If the ventilation velocity across the fire source becomes larger, the maximum excess temperature beneath the ceiling depends on both the heat release rate and the ventilation velocity. However, it also approaches a constant if the continuous combustion zone is present at the tunnel ceiling. In other words, if $V' > 0.19$ (Region II), the maximum excess temperature can be expressed as:

$$\Delta T_{\max} = \begin{cases} \mathrm{DTR\,II}, & \mathrm{DTR\,II} < 1350 \\ 1350, & \mathrm{DTR\,II} \geq 1350 \end{cases} \tag{32}$$

where the Delta T in Region II, DTRII, is defined as:

$$\mathrm{DTR\,II} = \frac{\dot{Q}}{u_o b_{fo}^{1/3} H_{ef}^{5/3}}$$

The above equation for maximum ceiling excess gas temperature can also be expressed in a simpler form:

$$\Delta T_{\max} = \min(\mathrm{DTR\,I}, \mathrm{DTR\,II},\ 1350) \tag{33}$$

Figure 24 shows a comparison of maximum ceiling excess gas temperatures measured in the tests and estimated using the above equations. All the test data for different ventilation conditions are plotted. Clearly, it shows that good agreement between the test data and the equations. It should be mentioned that the upper limit of 1000 °C for maximum excess gas temperature in the correlation instead of 1350 °C as used in the equations due to that it has been found in many model scale tests that the measured temperatures are slightly lower than those in full scale tests. This reason could also be responsible for the slight discrepancy for gas temperatures over 800 °C.

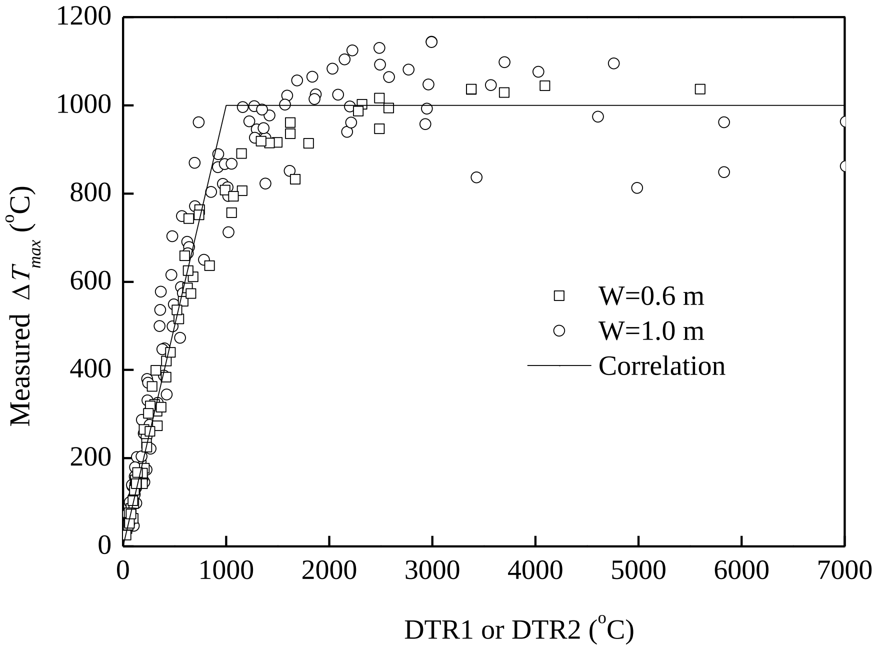

Figure 24 Comparison of maximum ceiling excess gas temperatures measured in the tests and estimated using the above equations.

Note that the above equations are used in estimation of the gas velocities of the ceiling jets under high ventilation, i.e. Eq. (23).

6.4.2 Ceiling temperature distributions along the tunnel

In large fires, the flames extend along the ceiling and continually release heat into the tunnel. This indicates that in the vicinity of the fire the gas temperatures could decrease much more slowly than further downstream. This phenomena has been observed by Ingason and Li [16]. In the analysis of test data from model scale tunnel fire tests and full scale tunnel fire tests conducted by SP, they found [16] that there is a virtual origin for large fires, that is, the gas temperatures between the fire source center and the virtual origin decrease very slowly. They proposed that this is due to the fact that the continuous flame continually introduces a large amount of heat into the smoke flow although the smoke flow releases heat along the tunnel.

Figure 25 shows an example of the dimensionless ceiling excess gas temperature along the tunnel as a function of x/H for test 803. Clearly, data for fires greater than 158 kW deviates from the curves for smaller fires. The offset distance can be extrapolated by an analysis of the temperature distributions shown in Figure 25. This offset distance is in reality the horizontal distance between the fire source center and the virtual origin. After consideration of the virtual origin, the dimensionless ceiling excess gas temperature along the tunnel is plotted as a function of $(x-x_v)/H$ for test 803 in Figure 26. Clearly, the test data correlate very well with an exponential fit line.

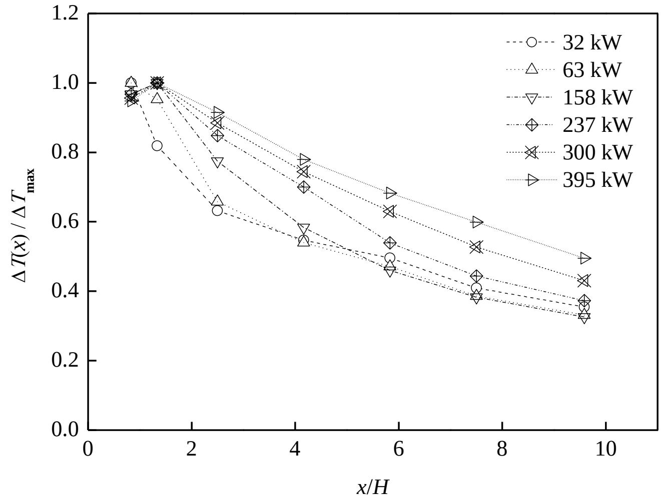

Figure 25 Dimensionless ceiling excess gas temperature along the tunnel as a function of x/H for test 803.

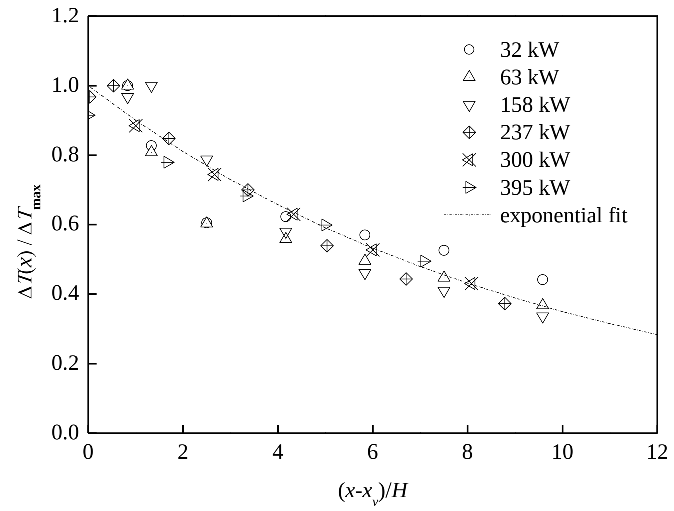

Figure 26 Dimensionless ceiling excess gas temperature along the tunnel as a function of $(x\text{-}x_v)/H$ for test 803.

Test data from the Runehamar tunnel fire tests conducted in 2003 [21] show similar trend. Figure 27 shows an example of the dimensionless ceiling excess gas temperature along the tunnel as a function of x/H for the Runehamar tunnel fire tests. Clearly, data for fires greater than 67 MW significantly deviates from the curves for smaller fires. After consideration of the virtual origin, the dimensionless ceiling excess gas temperature along the tunnel is plotted as a function of $(x\text{-}x_v)/H$ for the Runehamar tunnel fire tests in Figure 28. Clearly, the test data correlate very well with exponential fit line (sum of two exponential function).

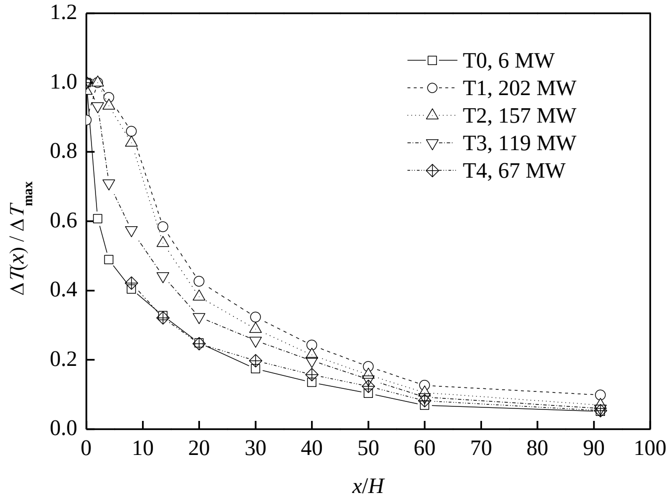

Figure 27 Dimensionless ceiling excess gas temperature along the tunnel as a function of x/H for the Runehamar tunnel fire tests.

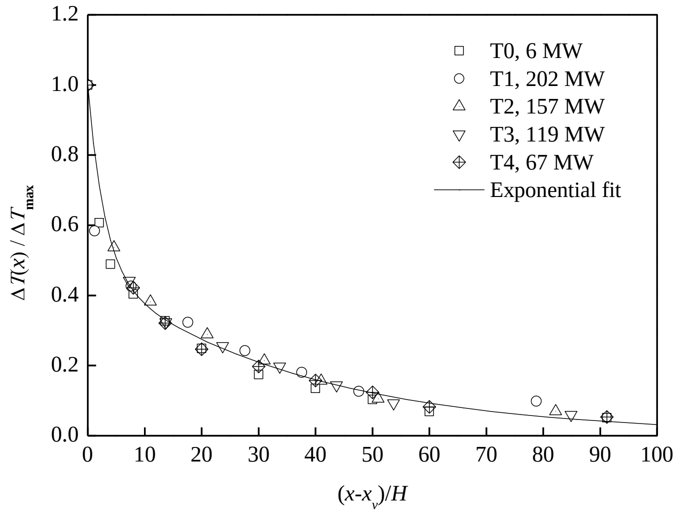

Figure 28 Dimensionless ceiling excess gas temperature along the tunnel as a function of $(x-x_v)/H$ for the Runehamar tunnel fire tests.

Based on the above analysis, it can be known that the virtual origin exists in large tunnel fires in both model scale and full scale, and the offset distance increases with the heat release rate.

6.4.2.1 High ventilation

The dimensionless ceiling excess gas temperature downstream of the fire for test series 7 under different velocities is plotted in Figure 29. The virtual origin is considered but the offset distance will be discussed later. It is shown in Figure 29 that the majority of test data lie beside the exponential fit. Further, no clear influence of ventilation velocity on the distribution of ceiling excess gas temperatures can be found, that is, this effect is negligible under high ventilation.

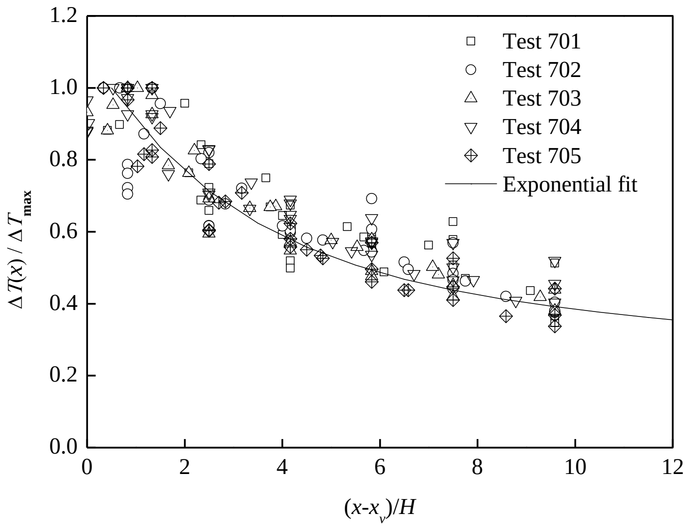

Figure 29 Distribution of dimensionless ceiling excess gas temperature along the tunnel for test series 7.

Data from full scale tunnel fire tests are also used in the following analysis. These full scale tests include the Runehamar tunnel tests conducted in 2003 [21], the Brunsberg tunnel tests in the Metro Project conducted in 2011 [33] and the Runehamar tunnel tests conducted in 2013 [34].

Figure 30 shows the dimensionless ceiling excess gas temperature downstream of the fire for both model scale and full scale tests. It is shown that all the experimental data correlates well with the sum of two exponential equations, which can be expressed as:

$$\frac{\Delta T(x)}{\Delta T_{\max}} = 0.53\exp(-0.34\frac{x-x_v}{H}) + 0.47\exp(-0.027\frac{x-x_v}{H}) \qquad (34)$$

where x_v is the offset distance between the virtual origin and the fire source (m).

In Figure 30 it is shown that the correlation underestimates the dimensionless temperature at x/H of 170 (1000 m downstream). The reason is that the exponential functions are only approximations rather than analytical solutions. Sum of more exponential functions will increase the accuracy while no effort is made for the simplicity of the correlations. For safety reasons, this equation is recommended to be used only for x/H less than 100 (approx. 500 m). For positions longer, the gas temperatures are very low and the one dimensional model is recommended, see the literature [26].

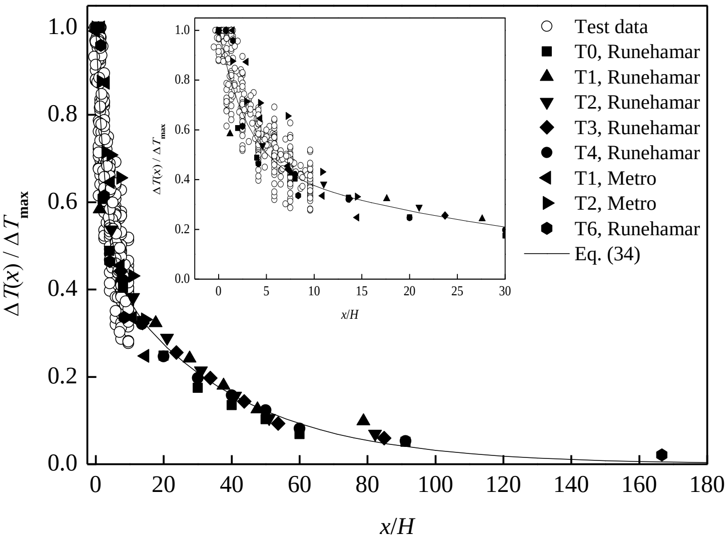

Figure 30 Distribution of dimensionless ceiling excess gas temperature along the tunnel for both model and full scale tests.

Note that a gas temperature of 500 to 650 ^{o}C could represent the temperature at a ceiling flame tip with an average value of 575 ^{o}C. A ceiling gas temperatures in a range of 600 ^{o}C to 1200 ^{o}C could correspond to the "intermittent flame region", that is, a less intense combustion region compared to the continuous flame region. On one hand, heat is continuously introduced to the smoke flow along the ceiling, which lessens the decrease in the ceiling gas temperature. On the other hand, this region corresponds to a higher heat transfer coefficient and more heat is lost in this region compared to the non-flaming region, which could aggravate the temperature decrease. However, Figure 30 shows that the ceiling gas temperature decreases more rapidly with distance in the vicinity of the fire than further away from the fire. In other words, the radiation loss still dominates within the intermittent flame region, as shown in Figure 30. It should, however, be kept in mind that between the fire source and the virtual origin the ceiling gas temperature decreases rather slowly with distance from the fire. The main reason is the introduction of a large amount of heat from the intense combustion within the "continuous flame region" balances the heat loss to a large extent. Within this range mainly from the maximum value of approx. 1350 ^{o}C (starting point of the continuous flame region) to approx. 1200 ^{o}C (at the edge of the continuous flame region). In case that the maximum value is lower, e.g. 1100 ^{o}C , the corresponding value for the edge of the continuous flame region could also be lower, e.g. 900 ^{o}C.

In the following the location of virtual origin is investigated and an estimation is made at first. As mentioned previously, the ceiling gas temperatures in a range of 600 ^{o}C to 1200 ^{o}C could correspond to the "intermittent flame region". According to the correlation for temperature distribution, the distance between a ceiling gas temperature of 1200 ^{o}C and 575 ^{o}C is approximately 5-6 times the tunnel height.

Figure 31 shows the dimensionless virtual origins as a function of the dimensionless flame lengths. Data from the Runehamar tunnel tests conducted in 2003 [21] are also plotted. Note that only hollow circular and solid circular points correspond to positive virtual origins. Clearly, both model and full scale test data for the offset distance between fire source center and virtual origin, x_v, can be well represented by a simple piecewise function:

$$x_v = \begin{cases} L_f - 5.2H, & L_f > 5.2H \\ 0, & L_f \le 5.2H \end{cases} \tag{35}$$

where L_f (m) is the flame length that can be estimated using equation proposed in Section 6.1.

Note that the value of 5.2 correlate very well with the theoretical estimation, i.e. a value between 5 to 6. This validates the theory, that is, the existence of the virtual origin is due to the introduction of a large amount of heat from the intense combustion within the "continuous flame region" that balances the heat loss to a large extent.

The above equation indicates that the virtual origin needs to be accounted for only when the fire is very large and the flame length is over 5.2 times the tunnel height. Otherwise, the virtual origin does not exist and can be considered as 0.

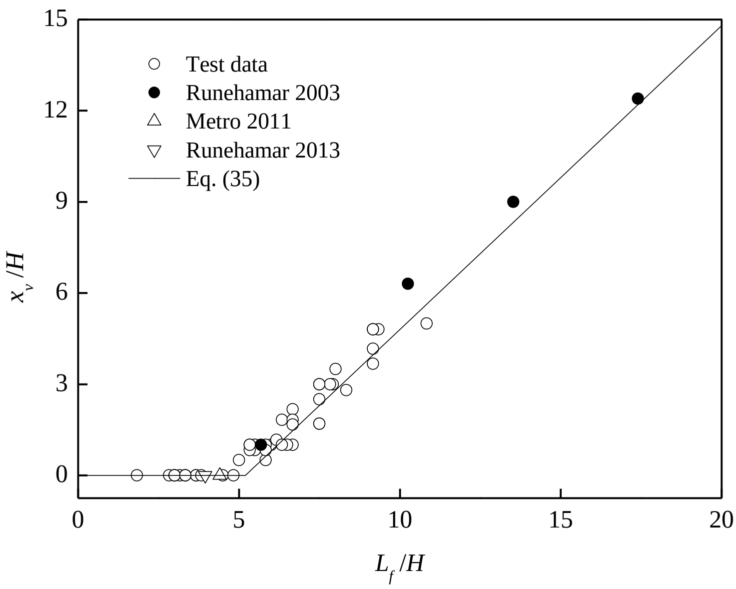

Figure 31 The virtual origin for large tunnel fires under high ventilation.

Note that in reality even for a small fire, high ventilation affects the position of maximum ceiling gas temperature and therefore affect the origin of the ceiling jet [20]. In most cases, this effect could be considered to be insignificant compared to the virtual origin due to long horizontal flames. The equation in [20] can be used if there is a need to estimated it. For rough estimation, the position of maximum ceiling temperature could be approx. 1.5 times effective tunnel height downstream for 3 m/s and 2.3 times for 6 m/s. Considerations of this effect may increase the accuracy of estimations.

6.4.2.2 Low ventilation or natural ventilation

Under natural ventilation, the smoke could flows out of both tunnel exits if no dominating flow direction exists. Therefore the scenarios are different with those under forced ventilation where smoke backlayering is prevented completely or the front of smoke backlayering is arrested.

For large fires under low ventilation, virtual origins exist on both sides of the tunnel.

The dimensionless ceiling excess gas temperature is plotted in Figure 32. Here the virtual origin is considered and the offset distance will be discussed later.

It is shown in Figure 32 that test data for natural ventilation are slightly lower than those for forced ventilation. This indicates that the smoke temperature decreases more rapidly under low ventilation. The main reason should be that under natural ventilation, the smoke flow rate on either side is much lower compared to that under forced ventilation. This phenomenon in fact can also be found for smoke reverse flows under high ventilation (with a certain backlayering).

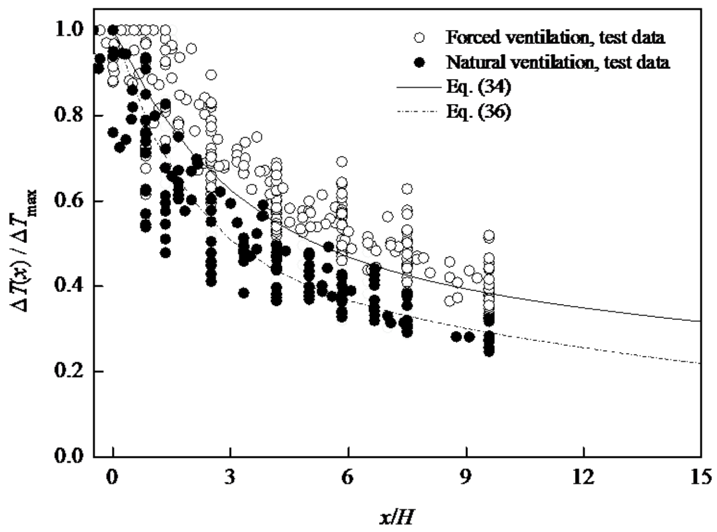

Figure 32 Distribution of dimensionless ceiling excess gas temperature along the tunnel under natural ventilation and forced ventilation.

Similarly, a sum of two exponential function is applied to fit the test data. The equation is expressed as:

$$\frac{\Delta T(x)}{\Delta T_{\max}} = 0.53\exp(-0.54\frac{x-x_v}{H}) + 0.47\exp(-0.05\frac{x-x_v}{H}) \qquad (36)$$

Note that test data correspond to x/H less than 10 (60 m in full scale). For safety reasons, this equation is recommended to be used only for x/H less than 10 (or a slightly greater value, e.g. 15 or 20). Test data further away from the fire are required for validation of the correlation.

This correlation could also be applied to estimate the temperature distribution for the smoke reverse flow upstream of the fire under high ventilation (with a certain backlayering). Generally the above equation produces conservative results for the smoke reverse flow.

In the following, the virtual origin under low ventilation is analysed. Figure 33 shows the the dimensionless virtual origins as a function of the dimensionless flame lengths.

Clearly, the same correlation for high ventilation can well represented the test data for natural ventilation. This means that Equation (35) can be used to determine the virtual origin for natural ventilated fires.

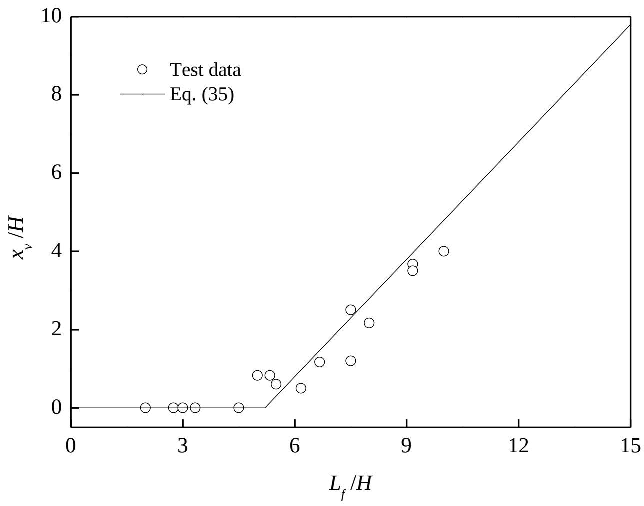

Figure 33 The virtual origin for large tunnel fires under natural ventilation.

6.5 Ceiling jet radiation

A theoretical model of smoke radiation is presented in Appendix D.

6.5.1 Radiation at ceiling

Figure 34 shows the incident radiation heat fluxes measured at the ceiling 1.5 m downstream of the fire site. At full scale, the location corresponds to 15 m downstream.

According to the theoretical analysis, the incident radiation heat flux at the ceiling can be directly correlated with ceiling gas temperatures, which can be expressed as follows:

$$\dot{q}''_{inc} = 0.85\sigma T_g^4 \quad (37)$$

The effective emissivity of 0.85 is determined from these model scale test data as shown in Figure 34.

Clearly, it can be seen that all the test data for both tunnels are closely following the correlations proposed. This verifies the reasonability of the theoretical model. Further, it indicates that in most tests the smoke flows are optically thick.

Also, note that at low heat fluxes, some measured heat fluxes are slightly below the line in Figure 34. This is due to the fact that these data points are mostly related to low heat release rates, as the effective emissivity for a small fire, e.g. 5 MW fire in a realistic tunnel, is lower than that for a large fire. However, the deviation is not as significant as what would be expected. This should be related to the heating of the whole tunnel structure.

Further, the tunnel width does not show significant influence on the incident heat fluxes at the ceiling.

Overall, the simple correlation shows excellent performance in collapse of all the test data from the model scale tests.

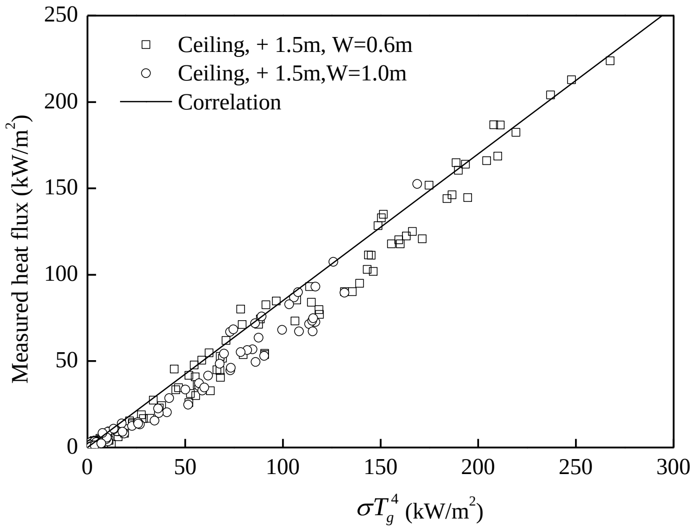

Figure 34 Radiation heat flux at the ceiling, 1.5 m downstream of the fire.

Note that the effective emissivity is slightly affected by scale of the scenario. In model scale tests, much less smoke particles are produced compared to corresponding full scale tests. A fully optically thick smoke in a model scale test is not as common as in a full scale test and therefore larger scale is always preferred but not always possible . For large tunnel fires, the gas emissivity, ε_g, can be assumed to be 1.

A comparison of the estimated incident heat fluxes by Eq. (D.5) (Eq. (37) with an emissivity of 1) and measured values in the Runehamar tunnel fire tests carried out in 2003 [31] is presented in Figure 35. All data lie close to the equality line which suggests a very good correlation.

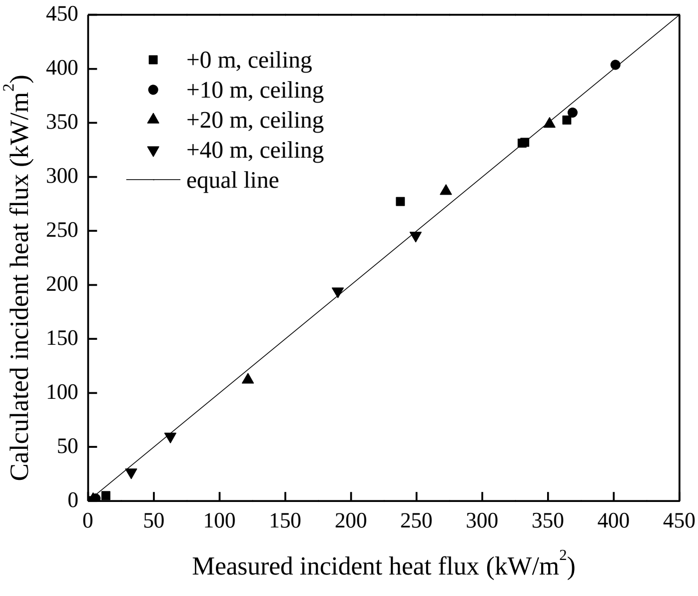

Figure 35 Comparison of calculated and measured incident heat fluxes in Runehamar tests.

In case that the emissivity of the smoke flow can be well estimated, a smaller effective emissivity can be used in estimation of ceiling incident heat fluxes. However, in most realistic tunnel fires, the smoke layer is very thick and behaves as a good radiation barrier (also a good radiation emitter). For engineering application, the emissivity should be assumed to be 1.

6.5.2 Radiation at floor

Figure 36 shows the incident radiation heat flux at the floor downstream of the fire. As the location is too close to the fire, data measured at 0.8 m downstream (8 m from the fire center at full scale) are not plotted here but will be discussed later.

The incident radiation heat flux received at the floor can be expressed as follows:

$$\dot{q}''_{inc} = 0.75\sigma T_g^4 \tag{38}$$

The value of 0.75 accounts for the effect of smoke emissivity, smoke layer height, view factor, and surrounding wall temperatures. If 50 % tunnel height is assumed as the smoke layer height, the corresponding view factors are 0.71 and 0.86 for tunnel width of 0.6 m and 1 m, respectively. These values correlate relatively well.

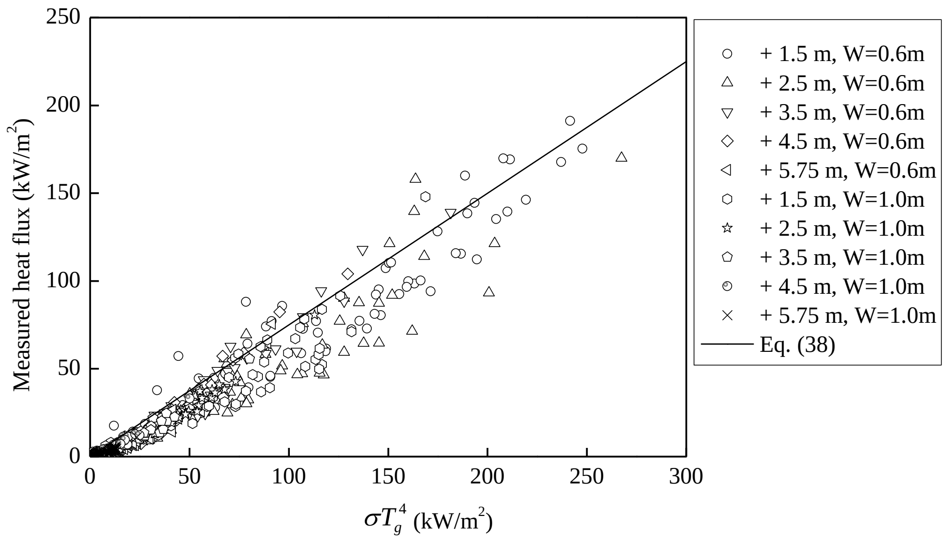

Figure 36 Incident radiation heat flux at the floor downstream of the fire (excluding +0.8 m).

Figure 37 shows the incident radiation heat flux at the floor downstream of the fire including the data measured at 0.8 m downstream of the fire center (solid points). It is shown that most test data measured at 0.8 m downstream correlate well with Eq. (38). However, some measured data are much higher than the line. After a careful examination of the data, it is found that most of these data correspond to the test with 3 m/s (9.4 m/s at full scale), where the fires are highly inclined and the location receives significant incident radiation directly from the combustion flame.

However, most data points are scattered closely to the correlation line.

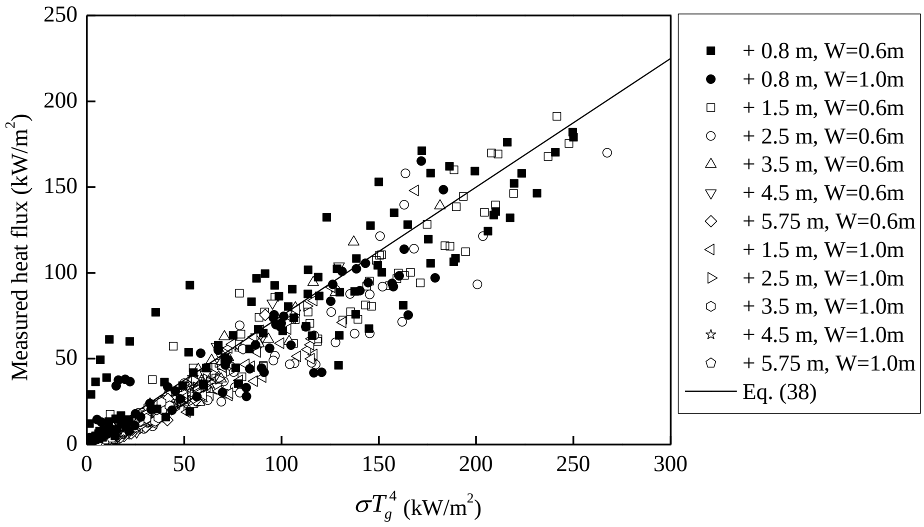

Figure 37 Incident radiation heat flux at the floor (including +0.8 m).

Figure 38 shows the incident radiation heat fluxes measured at 1 m upstream (-1.0 m) in comparison to those downstream of the fire. Note that the correlation for downstream is also applicable to that for upstream.

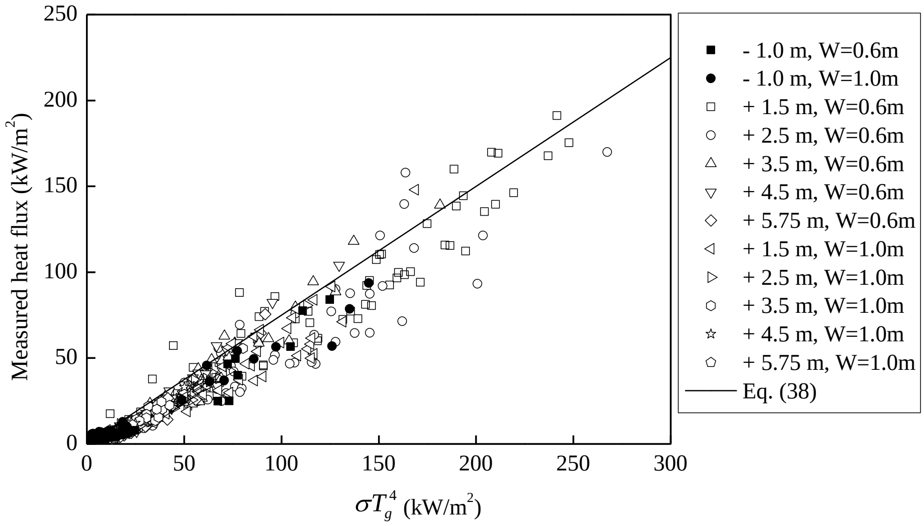

Figure 38 Incident radiation heat flux upstream (-1.0 m) and downstream at the floor level.

More test data are used to verify the model. Figure 39 shows a comparison of calculated and measured heat fluxes in the Runehamar tunnel fire tests [31]. The calculation are based on the equations proposed in Section 12.2. Data measured by seven heat flux meters are plotted in the figure. There were two heat flux meters placed 20 m from the fire beside a pallet pile (the object), with one heat flux meter facing the fire and another flush with the wall facing the object. All heat flux meters were placed 1.6 m above the tunnel floor with the exception of the one at 10 m which was placed on the floor. Only the heat flux meter placed at 20 m facing the fire was a plate thermometer (PT) measuring incident heat flux. The others were Schmidt Boelter gauges measuring net heat fluxes using water cooling of the surface of the probe. An emissivity of 0.9 for the Schmidt Boelter gauges was assumed. For the heat flux meter at 0 m it can be assumed that this heat flux meterwas surrounded by the flames and thus a view factor of 1 was used in the calculations. Further, the view factor for the two heat flux meters at 20 m can also expected to be 1 since the large object also placed at 20 m was burning during the tests. The heat fluxes measured at 20 m increased significantly when the object started to burn. For all the other positions, it was assumed that the characteristic upper smoke layer was at 50 % of the tunnel height. The flames were very sooty and the emissivity was assumed to be 1 for all the tests. Note that this assumption works in most engineering applications while estimating the heat fluxes although it could result in slightly conservative values for small fires. For heat flux meters facing fire, heat flux from the upper smoke layer and from the vertical flame section were superposed as the total heat flux.

It is shown in Figure 39 that most of data points fall in the vicinity of the equality line, which suggests that the measured and calculated heat fluxes correlate reasonably well.

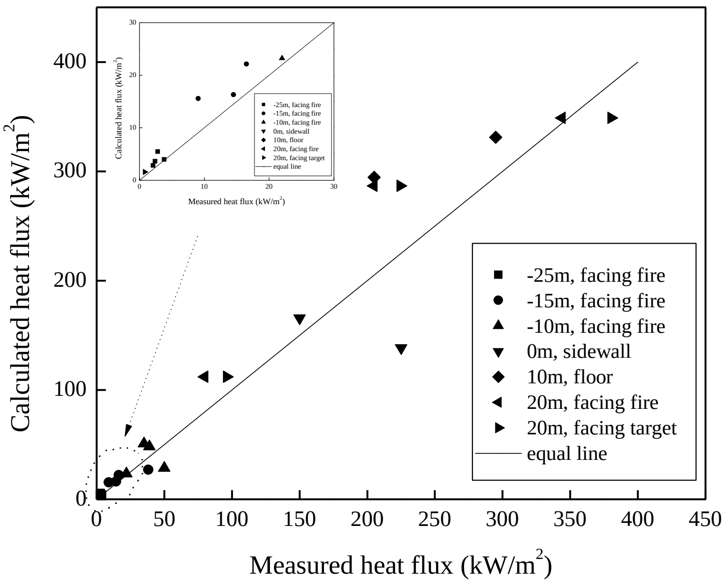

Figure 39 Comparison of measured heat fluxes and calculated values in Runehamar tunnel tests.

Figure 40 shows the comparison of calculated and measured heat fluxes in model scale tests with longitudinal [16] and point extraction ventilation [22]. The heat fluxes were measured by SB gauges placed on the tunnel floor. The aspect ratio, i.e. ratio of width to height, of the tunnel tested was 1.5 and 2.0. In these tests, the flames were very sooty so the emissivity is assumed to be 1 for all the tests. The characteristic upper smoke layer was assumed to be at 50 % of tunnel height. Figure 40 shows that the calculated heat fluxes correlate very well with the measured values.

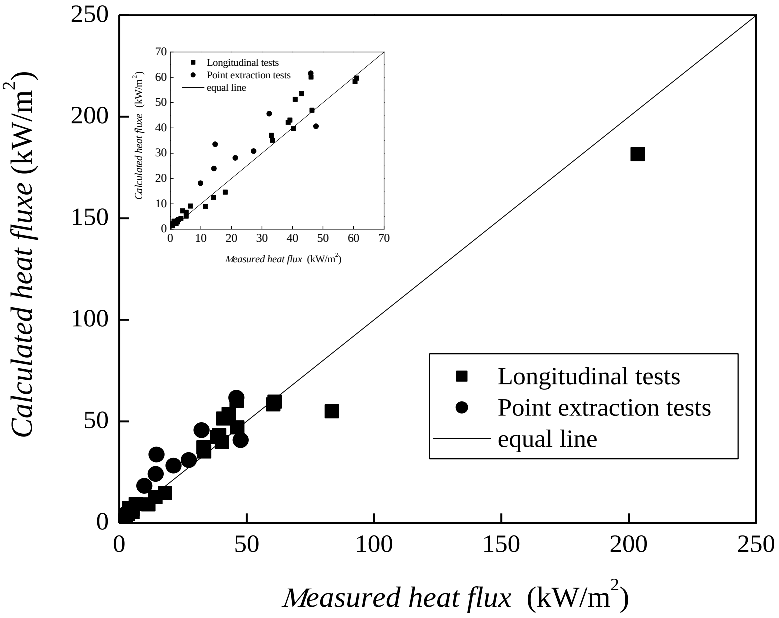

Figure 40 Comparison of measured and calculated heat fluxes in model scale fire tests.

6.6 Fire spread

The ignition time for both wood and plastic targets is summarized in Table 3.

Figure 41 shows the measured heat fluxes with and without ignition of wood targets as a function of longitudinal velocity. Note that the heat release rates were increased step by step in the tests. This results in sharp increase in the heat fluxes during the changing period. The data with and without ignition of targets may thus scatter significantly. Therefore it is not expected to measure accurately the critical heat fluxes for fire spread in the tests. However, it is shown in Figure 41 that most data with ignition is above around 20 kW/m^2 (solid points) and those without ignition (hollow points) below it. Therefore, it could be concluded that the critical heat flux for fire spread to wood targets at lower layer is approximately 20 kW/m^2.

Careful examination of the test data indicates a minimum critical heat flux of around 12.5 kW/m^2 in the tests with natural ventilation. There could be a trend that the critical heat flux increases slightly with ventilation velocity. One reason could be that more convective heat loss occurred under higher ventilation. This trend could be more obvious between 0 m/s and 0.5 m/s where the flow patterns are completely different.

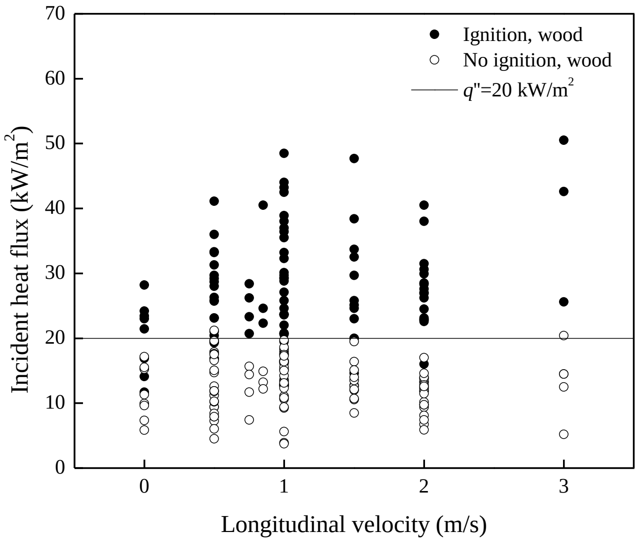

Figure 41 Ignition criterion for wood targets.

Figure 42 the measured heat fluxes with and without ignition of plastic targets as a function of longitudinal velocity. Similar distinction between the data points with and without ignition can be found in this figure. The critical heat flux under tested conditions is also approximately 20 kW/m^2. At the early stage, it could also be found that the critical heat flux increases slightly with the velocity.

Although both figures show a critical heat flux of 20 kW/m^2, the behaviours of wood and plastic targets were very different in cases with high ventilation. Under high ventilation, significant amounts of vaporized gases can be produced from plastic targets but they could be blown away by wind and all consumed before any possible ignition. This should be due to the low pyrolysis temperature and low heat of pyrolysis of the HDPE. Note that the sample is quite thin. In cases that much thicker plastic targets were placed they could be ignited at the end.

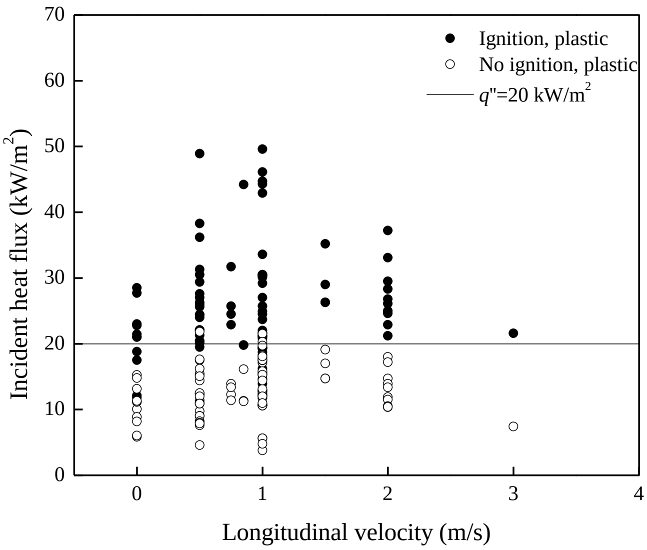

Figure 42 Ignition criterion for plastic targets.

The fire point equation can be used to identify the state of ignition. It could be reasonably assumed that the heat conduction between the pyrolysis layer and the deeper layer is negligible, compared to the other terms in the fire point equation. This should be reasonable after the target has been exposed to the hot environment for a certain time. Therefore net heat flux on the fuel surface at the ignition can be expressed as:

$$\dot{q}''_{net} = \alpha \dot{q}''_{inc} - \alpha \sigma T_{ig}^4 - h_c (T_{ig} - T_g) - \dot{m}''_f L_p \qquad (39)$$

where $\dot{m}''_f$ is the critical burning rate for sustaining a steady flame, L_p is heat of pyrolysis (including enthalpy term).

Note that in order to ignite a target, the net heat flux at the ignition should not be less than 0. All the test data have been checked and approximately fulfill this requirement. The average net heat flux (excluding the critical evaporation term, $\dot{m}''_f L_p$) is in a range of 5 to 7.5 kW/m^2. This value can be attributed to the combined effect of the evaporation term, $\dot{m}''_f L_p$, and the heat conduction loss term that is ignored in Eq. (39). Note that both the convection term and the pyrolysis term are related to local velocity.

The range of ignition in tests with different ventilation conditions is also investigated. The basic finding is that high ventilation reduces the risk for fire spread. The main reason is that under high ventilation the gas temperature is slightly lower but results in a much lower radiation heat flux given that the heat flux varies as 4th power of the absolute gas temperature.

The criteria found for ignition should be applicable to full scale tunnels. In tests it was found that the targets were ignited only after the flame existed above the target. However, it should be noted that the heat flux scales as ½ power of the length scale. Therefore the heat fluxes at ignition in the tests correspond to much higher heat fluxes at full scale. This indicates in full scale the region that fire spread could occur should be longer than the one obtained from model scale (even when the region length has been scaled up).

Table 3 Ignition time in the tests (unit: min).

Test no.	**Target 1**		**Target 2**		**Target 3**		**Target 8**		**Target 4**		**Target 5**		**Target 6**		**Target 7**	
	W[a]	P[b]	W[a]	P[b]	W[a]	P[b]	W[a]	P[b]	W[a]	P[b]	W[a]	P[b]	W[a]	P[b]	W[a]	P[b]
101	23.2	-	27.0	-	Charred	-	-	-	-	-	-	-	-	-	-	-
102	-	-	26.0	-	-	-	Charred	-	-	-	-	-	-	-	-	-
103	-	24.2	24.4	-	26.8	-	-	26.7	-	-	-	-	-	-	-	-
104	21.6	23.2	23.2	24.5	25.6	25.7	25.6	26.1	Red[c]	-	-	-	-	-	-	-
105	0.8	-	2.0	-	5.2	-	5.0	2.7	7.0	10.6	Charred	-	-	-	-	-
106	0.8	-	1.3	-	1.8	-	1.6	1.6	3.4	5.1	5.7	5.7	6.5	7.3	-	-
201	21.9	-	24.0	-	Charred	-	-	-	-	-	-	-	-	-	-	-
202	21.9	-	23.8	-	27.8	-	-	-	-	-	-	-	-	-	-	-
203	20.4	-	24.1	24.5	25.2	26.4	25.4	26.4	-	-	-	-	-	-	-	-
204	21.2	-	24.0	24.3	25.2	25.6	25.2	25.6	Red[c]	-	-	-	-	-	-	-
205	1.1	-	1.7	2.5	3.8	-	1.8	5.2	6.3	6.1	7.3	13.3	-	13.3	-	-
207	21.1	20.3	22.0	24.0	25.6	25.1	25.2	24.9	28.1	28.5	-	-	-	-	-	-
301	25.5	-	-	26.8	-	-	-	-	-	-	-	-	-	-	-	-
302	22.1	-	24.5	25.0	26.8	26.4	26.9	26.4	-	-	-	-	-	-	-	-
303	2.1	2.1	1.9	-	4.2	-	2.3	-	5.7	6.1	8.9	-	9.4	10.1	-	-
401	-	22.0	26.8	-	-	-	28.3	-	-	-	-	-	-	-	-	-
402	23.9	21.6	24.5	-	27.3	26.8	25.1	26.8	-	-	-	-	-	-	-	-
405	-	<20.6	24.4	24.6	27.2	25.7	26.3	25.6	-	-	-	-	-	-	-	-
403	1.8	1.0	1.9	-	4.1	3.2	1.7	3.2	6.6	6.9	7.5	8.2	-	-	-	-
501	20.3	20.1	21.6	21.8	25.4	25.0	25.5	24.7	28.5	28.5	-	-	-	-	20.4	19.5
502	NI	16.6	NI	-	23.2	23.0	22.8	22.7	-	-	-	-	-	-	-	-
601	16.7	18.2	-			24.9	-	24.7	-	-	-	-			<18.4	<18.4
602	17.5	17.2	NI	19.5	22.4	22.4	22.5	22.2	-	-	-	-			<19.8	-
603	1.0	-	1.6	1.8	3.5	3.5	2.4	3.3	4.5	5.3	5.9	6.1	-	-	9.6	9.6
701	18.1	-	-	-	24.5	24.9	21.4	22.5	27.0	-	-	-	-	-	-	-
702	17.9	17.0	19.4	-	22.9	21.9	20.8	21.9	24.8	25.4	26.7	-	-	-	-	-

703	16.0	16.0	18.5	18.5	<21.9	19.7	19.5	19.5	NA	22.6	NA	23.2	NA	25.3	-	-
704	15.7	16.0	18.3	18.2	19.6	19.3	18.6	18.7	21.5	21.3	22.4	22.2	26.0	25.8	-	-
705	15.6	15.9	18.1	17.9	19.0	18.7	18.4	18.5	<21.3	<21.3	B	B	-	-	-	-
801	18.3	-	19.3	-	22.7	22.6	21.5	22.6	26.1	-	26.6	-	-	-	-	-
802	16.9	17.0	18.8	-	21.2	21.6	NI	-	23.5	-	26.3	-	-	-	-	-
803	15.5	16.3	18.3	-	19.6	19.5	19.1	18.8	NI	23.4	23.6	25.7	26.6	26.7	-	-
804	15.8	16.4	17.8	-	20.1	20.1	19.9	19.1	22.1	22.1	23.1	22.6	24.7	24.7	-	-
805	16.5	-	18.3	18.7	18.7	18.9	18.3	18.3	21.5	20.9	22.1	22.3	26.7	25.9	-	-
901	Pilot	<15.6	21.4	-	25.0	-	21.3	-	26.8	-	-	-	-	-	-	-
902	-	<18.3	19.6	-	23.1	22.1	19.9	21.6	25.6	25.8	-	-	-	-	-	-
903	16.0	15.8	18.7	18.7	21.3	20.4	19.5	20.0	<23.9	<23.9	24.6	<24.5	25.1	25.1	-	-
904	15.7	<16.5	18.2	18.2	19.2	19.1	18.7	18.8	21.8	21.8	24.6	24.3	Critical	27.0	-	-
905	<	0.7	0.7	1.0	1.1	1.2	0.6	0.9	1.2	1.5	2.7	3.1	3.3	3.3	-	-
1,001	18.5	18.5	19.9	23.1	23.0	23.8	21.6	22.9	25.8	-	-	-	-	-	-	-
1,002	15.8	15.9	18.2	18.3	20.0	19.4	19.0	19.0	22.1	22.2	25.2	23.5	24.3	24.8	-	-

[a] Wood . [b] Plastic. [c] Visibly red, close to ignition.

7 Summary

Theoretical analyses and experimental work were carried out to investigate the ceiling jet characteristics in tunnel fires. A series of fire tests was carried out in two model tunnels with a scaling ratio of 1:10. The parameters tested include heat release rate, ventilation velocity, fire source height and tunnel geometry. The key ceiling jet characteristics parameters focused on are flame lengths, ceiling jet velocity, ceiling jet mass flow rate, gas temperatures, radiation and fire spread.

A theoretical model of flame lengths in tunnels is proposed and validated using test data. Under low ventilation, i.e. dimensionless velocity $u^*<0.3$, there exists both upstream flame and downstream flame, and the upstream flame length decreases linearly with the increasing velocity. Under high ventilation, $u^*>0.3$, only downstream flame exists. Regardless of ventilation velocity, the downstream flame length increases linearly with the heat release rate, and decreases with tunnel width and effective tunnel height. The total flame length can be as long as twice the downstream flame lengths. Correlations for downstream flame lengths, upstream flame lengths, and total flame lengths are proposed.

Theoretical model of ceiling jet velocity in tunnels under different ventilation conditions is proposed and validated using test data. Under natural ventilation, the ceiling jet velocity increases with heat release rate and decreases with effective tunnel height. Under forced ventilation, the ceiling jet velocity increases with the ventilation velocity and the ceiling jet temperature.

The mass flow rate of the fire plume increases with heat release rate and effective tunnel height, under natural ventilation. Under high ventilation, the smoke mass flow rate increases linearly with ventilation velocity, independent of heat release rate. Correlations for the ceiling jet mass flow rate under different ventilation are proposed.

Theoretical analysis of distribution of gas temperature of the ceiling jet in a tunnel fire is presented. It has been found that there are virtual origins for large tunnel fires and the gas temperatures between the fire source center and the virtual origin decrease very slowly. This is due to the large amount of heat released within the ceiling intensive combustion region. Correlations for both the ceiling gas temperatures and the virtual origins under low and high ventilation are proposed.

Theoretical models of radiation heat fluxes in small and large tunnel fires are presented and verified using test data. The tunnel surfaces in the upper smoke layer are surrounded by smoky gases and/or flames in a large fire. The incident heat flux in the upper smoke layer can be simply correlated with the smoke temperature and the emissivity of the smoke volume. For large fires, the emissivity can be assumed to be 1. To calculate the incident heat flux in the lower layer, the view factor must be accounted for, together with the upper layer smoke temperature and the emissivity of the smoke volume.

Fire spread occurred when the radiation heat flux is greater than approximately 20 kW/m^2. The net heat flux on the fuel surface at the ignition is found to be a positive value.

8 References

1. *Thematic Network on Fires in Tunnels (FIT) - Technical Report Part 1 - Design Fire Scenarios* 2001 - 2004, European Commission under the 5th Framework Program
2. Ingason H, *Design fire curves in tunnels.* Fire Safety Journal, 2009. **44**(2): p. 259-265.
3. Ingason H. *Design fire in tunnels*. in *Safe & Reliable Tunnels Innovative European Achievements, Second International Symposium*. 2006. Lausanne.
4. Li YZ, Ingason H, *A new methodology of design fires for train carriages based on exponential curve method.* Fire Technology, 2015.
5. Kennedy W. D. *Critical velocity: Past, Present and Future*. in *Seminar of Smoke and Critical Velocity in Tunnels*. 1996. London: JFL Lowndes, 1996, pp.305-322: JFL Lowndes.
6. Wu Y, Bakar MZA, *Control of smoke flow in tunnel fires using longitudinal ventilation systems - a study of the critical velocity.* Fire Safety Journal, 2000. **35**: p. 363-390.
7. Li YZ, Lei B, Ingason H, *Study of critical velocity and backlayering length in longitudinally ventilated tunnel fires.* Fire Safety Journal, 2010. **45**: p. 361-370.
8. Li YZ, Lei B, Ingason H, *The maximum temperature of buoyancy-driven smoke flow beneath the ceiling in tunnel fires.* Fire Safety Journal, 2011. **46**(4): p. 204-210.
9. Li YZ, Ingason H, *The maximum ceiling gas temperature in a large tunnel fire.* Fire Safety Journal, 2012. **48**: p. 38-48.
10. Li YZ, Ingason H, *Maximum Temperature beneath Ceiling in a Tunnel Fire*, 2010, SP Report 2010:51, SP Technical Research Institute of Sweden.
11. Rew C, Deaves D. *Fire spread and flame length in ventilated tunnels - a model used in Channel tunnel assessments*. in *Proceedings of the International Conference on Tunnel Fires and Escape from Tunnels*. 1999. Lyon, France: Independent Technical Conferences Ltd.
12. *Fires in Transport Tunnels: Report on Full-Scale Tests*, 1995, edited by Studiensgesellschaft Stahlanwendung e. V.: Düsseldorf, Germany.
13. *Memorial Tunnel Fire Ventilation Test Program - Test Report*, 1995, Massachusetts Highway Department and Federal Highway Administration.
14. Lönnermark A, Ingason H, *Fire Spread and Flame Length in Large-Scale Tunnel Fires.* Fire Technology, 2006. **42**(4): p. 283-302.
15. Alpert RL, *Ceiling Jet Flows*, in *SFPE Handbook of Fire Protection Engineering*, PJ DiNenno, Editor 2002, National Fire Protection Association: Quincy, MA, USA. p. 2-18 -- 2-31.
16. Ingason H, Li YZ, *Model scale tunnel fire tests with longitudinal ventilation.* Fire Safety Journal, 2010. **45**: p. 371-384.
17. Heskestad G, Hamada T, *Ceiling Jets of Strong Fire Plumes.* Fire Safety Journal, 1993. **21**: p. 69-82.
18. Hinkley PL, *The Flow of Hot Gases Along an Enclosed Shopping Mall - A Tentative Theory*, 1970, Fire Research Station.
19. Li S., Zong R., Zhao W., Yan Z., Liao G., *Theoretical and experimental analysis of ceiling-jet flow in corridor fires.* Tunnelling and Underground Space Technology, 2011. **26**: p. 651-658.
20. Li YZ, Ingason H, *Position of maximum ceiling temperature in a tunnel Fire.* Fire Technology, 2014. **50**: p. 889–905.
21. Ingason H, Li YZ, Lönnermark A, *Runehamar Tunnel Fire Tests.* Fire Safety Journal, 2015. **71**: p. 134–149.
22. Ingason H, Li YZ, *Model scale tunnel fire tests with point extraction ventilation.* Journal of Fire Protection Engineering, 2011. **21**(1): p. 5-36.

23. Newman JS, Tewarson A, *Flame Propagation in Ducts.* Combustion and Flame, 1983. **51**: p. 347-355.
24. Li YZ, Ingason H. *The fire growth rate in a ventilated tunnel fire*. in *10th International Symposium on Fire Safety Science (IAFSS)*. 2011. Maryland, USA.
25. Li YZ, Hertzberg T, *Scaling of internal wall temperatures in enclosure fires.* Journal of Fire Science, 2015. **33**(2): p. 113-141.
26. Ingason H, Li YZ, Lönnermark A, *Tunnel Fire Dynamics*2015, New York: Springer.
27. Janssens M, Tran HC, *Data Reduction of Room Tests for Zone Model Validation.* Journal of Fire Sciences, 1992. **10**(November/December): p. 528-555.
28. McGrattan K, Klein B, Hostikka S, Floyd J, *Fire Dynamics Simulator User Guide (Version 6)* 2013, National Institute of Standards and Technology: USA.
29. Schlichting H, *Boundary-layer theory*. 7th ed1979, New York: McGraw-Hill.
30. McCaffrey BJ, *Purely Buoyant Diffusion Flames: Some Experimental Results*, 1979, National Bureau of Standards: Washington, D.C., USA.
31. Ingason H, Lönnermark A, Li YZ, *Runehamar Tunnel Fire Tests*, 2011, SP Technicial Research Institute: SP Report 2011:55.
32. Hinkley PL, Wraight HGH, Theobald CR, *The Contribution of Flames under Ceiling to Fire Spread in Compartments.* Fire Safety Journal, 1984. **7**: p. 227-242.
33. Lönnermark A, Lindström J, Li YZ, Claesson A, Kumm M, Ingason H, *Full-scale fire tests with a commuter train in a tunnel*, in *SP Report 2012:05*2012, SP Technical Research Institute of Sweden: Borås, Sweden.
34. Ingason H, Li YZ, Appel G, Lundström U, Becker C, *Large scale tunnel fire tests with large droplet water-based fixed fire fighting system.* Fire Technology, 2015.
35. Delichatsios MA, *Air Entrainment into Buoyant Jet Flames and Pool Fires.* Combustion and Flame, 1987. **70**: p. 33-46.
36. Thomas PH. *The Size of Flames from Natural Fires*. in *9th Int. Combustion Symposium*. 1963. Pittsburg, PA: Comb. Inst.
37. Bailey JL, Forney GP, Tatem PA, Jones WW, *Development and Validation of Corridor Flow Submodel for CFAST.* Journal of Fire Protection Engineering, 2002. **12**(3): p. 139-161.
38. Kunsch JP, *Simple model for control of fire gases in a ventilated tunnel.* Fire Safety Journal, 2002. **37**: p. 67-81.
39. Hamilton DC, and Morgan WR, *Radiant-interchange configuration factors*, 1952, NASA.
40. Chung BTF, Kermani MM, *Radiation view factors from a finite rectangular plate.* Journal of Heat Transfer, 1989. **111**(4): p. 1115-1117.

9 Appendix A – Theoretical model of flame lengths

A simple theoretical model of flame lengths in tunnel fires is proposed and described in the following.

9.1 Model of flame length in tunnel fires

Under low ventilation rate conditions, two parts of the flame exist: upstream and downstream of the fire, respectively.

In the ceiling flame zone, relatively good stratification mostly exists, that is, there is a clear layer interface between the fire and the fresh air. At the flame tip, the mass flow rate entrained in the horizontal combustion region can be estimated as follows:

$$\dot{m}_{hr} = \int_0^{L_f} \rho_o v W dx \qquad \text{(A.1)}$$

where $\dot{m}_{hr}$ is the mass flow rate of the entrained air from the lower layer by the horizontal flame (kg/s), ρ_o is the density of the entrained air (kg/m^3), v is the entrainment velocity (m/s), W is tunnel width (m), x is distance from the fire and L_f is the horizontal flame length (m).

The combustion in the horizontal flame is mainly dependent on the entrainment of the air flow and the mixing at the interface. The entrainment velocity for the mixing layer is given in the same form as that for the vertical plume. The upstream and downstream entrainment rates, can be expressed as:

$$v_{us} = \beta\left|u_{us} + u_l\right|, \quad v_{ds} = \beta\left|u_{ds} - u_l\right| \qquad \text{(A.2)}$$

where subscripts *us* and *ds* represent upstream and downstream, respectively, "+" indicates opposite directions between longitudinal flow and smoke, and vice versa. Subscript *l* indicates lower layer. Note that the entrainment coefficient in a vertical plume is assumed to be a constant. For simplicity, we also assume the average entrainment coefficient along the flame, β, is a constant.

Thus the mass flow rate of total entrained air downstream, $\dot{m}_{ds}$ (kg/s), and upstream of the fire, $\dot{m}_{us}$ (kg/s), can be respectively expressed as:

$$\dot{m}_{ds} = \rho_o v_{ds} W L_{f,ds}, \quad \dot{m}_{us} = \rho_o v_{us} W L_{f,us} \qquad \text{(A.3)}$$

We also know from the research on open fires that there is a relationship between the heat release rate and the entrained air, that is, the heat release rate should be intimately related to the mass of entrained air flows. Here we assume that the ratio of air flows involved in reaction and total entrained air flows is ξ. Therefore, the energy equation can be expressed as:

$$\dot{Q} = \dot{Q}_{vt} + (\xi_{ds}\dot{m}_{ds}Y_{O_2,ds} + \xi_{us}\dot{m}_{us}Y_{O_2,us})\Delta H_{O_2} \qquad \text{(A.4)}$$

where $\dot{Q}_{vt}$ is the heat released in the vertical flame region (kW), ξ is the ratio of the oxygen involved in the combustion to the oxygen entrained (or the ratio of air flow involved in the combustion to the total entrained air flow), ΔH_{O2} is the heat released while consuming 1 kg of oxygen (kJ/kg), Y_{O2} is the mass concentration of oxygen in the air flow at the lower layer. The second term on the right-hand side means the heat released in the horizontal flame regions. Note that although the parameter ξ for horizontal ceiling flames has the same physical meaning as that for open fires, the values could be different.

Inserting Eq. (A.10) into Eq. (A.11) gives:

$$\dot{Q} = \dot{Q}_{vt} + (\xi_{ds}\rho_o W L_{ds} \beta Y_{O_2,ds} \left| u_{ds} - u_o \right| + \xi_{us}\rho_o W L_{us} \beta Y_{O_2,us} \left| u_{us} + u_o \right|) \Delta H_{O_2} \qquad \text{(A.5)}$$

For upstream and downstream ceiling flames, the ratio ξ should be approximately the same, i.e. $\xi_{ds} = \xi_{us} = \xi$. Therefore, we have

$$L_{f,ds} Y_{O_2,ds} (u_{ds} - u_l) + L_{f,us} Y_{O_2,us} (u_{us} + u_l) = \frac{\dot{Q} - \dot{Q}_{vt}}{\xi \rho_o \beta W \Delta H_{O_2}} \qquad \text{(A.6)}$$

The mass flow rate in the vertical flame region under different ventilation conditions has not yet been explored thoroughly. Li et al. [8, 9] carried out a theoretical analysis of the maximum gas temperature beneath a tunnel ceiling and the mass flow rate of the fire plume in a ventilated flow based on a plume theory. However, the entrainment of the flame zone is very different compared to the plume zone. Due to lack of information we may assume that the entrainment inside the flame region in tunnel flows is similar to that in open fires. Delichatois [35] proposed simple correlations for the mass flow rate inside the flame:

$$\dot{m}(z) \propto D_F^2 z^{1/2} \quad \text{for } z / D_F < 1 \qquad \text{(A.7)}$$

where z is height above the fire source (m), $\dot{m}(\mathrm{z})$ is the mass flow rate inside the flame at height z (kg/s), and D_F is the diameter of the fire source (m). Note that the equation for the mass flow at height z can also be expressed as:

$$\dot{m}(\mathrm{z}) \propto \rho u D(\mathrm{z})^2 \qquad \text{(A.8)}$$

where u is vertical gas velocity (m/s) and $D(z)$ is diameter of the plume at height z (m). It can be expected that the fire plume diameter is proportional to the diameter of the fire source, i.e. $D(z) \propto D_F$, and the temperature inside the continuous flame zone can be reasonably considered as constant. Combing the above two equations suggests that the maximum vertical gas velocity, $u_{max,v}$, can be expressed as:

$$u_{\max,v} \propto H_{ef}^{1/2} \qquad \text{(A.9)}$$

where $u_{max,v}$, is the maximum velocity of the vertical flame (m/s), H_{ef} is the effective tunnel height (m), i.e. the tunnel height above the fire source. For vehicle fires or solid fuel fires, the effective tunnel height is the vertical distance between the bottom of the fire source and the tunnel ceiling. The above relationship correlates well with Thomas' equation for gas velocities in the flame zone [36].

The velocity of the fire plume after impingement on the ceiling slightly decreases, however, it can be assumed to be proportional to the maximum velocity in the vertical plume, as proved in the research on ceiling jets [15]. This indicates the maximum horizontal gas velocity, $u_{max,h}$, could also be expressed as:

$$u_{\max,h} \propto H_{ef}^{1/2} \tag{A.10}$$

where $u_{max,h}$ is the maximum velocity of the horizontal flame (m/s). This velocity could be considered as a characteristic velocity for the ceiling flames.

9.2 Flame length under high ventilation

The high ventilation here corresponds to the ventilation velocity under which no ceiling flame exists upstream of the fire source. In such cases, the ceiling flames only exist downstream of the fire, see Figure 43.

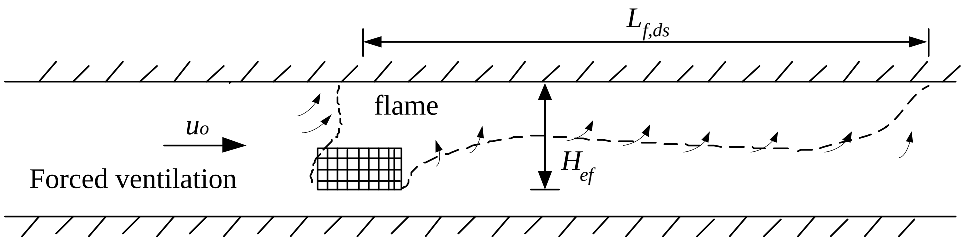

Figure *43* *A schematic diagram of entrainment under high ventilation.*

Note that generally the longitudinal ventilation velocity is around 3 m/s for a tunnel with longitudinal ventilation during a fire. In contrast, for a large tunnel fire with a relatively long ceiling flame length, the smoke velocity right above the fire could range from 5 to 10 m/s or even higher. This velocity appears to be much higher than the longitudinal ventilation velocity. However, the actual gas velocity at the lower layer in a large tunnel fire is significantly higher than the longitudinal ventilation velocity, and therefore the difference in gas velocities between the two layers is not as significant as expected. One reason is that the air has been heated up to a significant degree by the flames, hot smoke and tunnel surfaces before it is entrained. Another reason is the blockage effect caused by the fire source and hot gases. Therefore we may use the gas velocity under natural ventilation to approximately express the velocity difference between the ceiling flame layer and lower layer, that is

$$u_{ds} - u_l \propto H_{ef}^{1/2} \tag{A.11}$$

For a HGV fire, the horizontal flame could be very long, i.e. several times or even over ten times the tunnel height. The combustion in the vertical flame region could be limited due to the confinement of the tunnel configuration. Moreover, the flame was deflected and thus the vertical flame region also contributes to the flame length. Therefore, as a first attempt, the combustion in the vertical flame region is ignored. Given that the air entrained from the lower layer is generally not highly vitiated, the oxygen concentration for the entrained air is considered to be constant, i.e. close to ambient. Thus from Eq. (A.13) one gets:

$$L_{f,ds} = \frac{\dot{Q}}{\xi \rho_o \beta \Delta H_{O_2} Y_{O_2} W H_{ef}^{1/2}} \propto \frac{\dot{Q}}{W H_{ef}^{1/2}} \tag{A.12}$$

For a rectangular tunnel, $A=WH$. For other shapes, the tunnel width could vary with the flame layer height above the floor. For simplicity, let us estimate the tunnel width using $W=A/H$. The above equation can therefore be written as:

$$L_{f,ds} \propto \frac{\dot{Q}H}{AH_{ef}^{1/2}} \tag{A.13}$$

9.3 Flame length under low ventilation

Under low ventilation rate conditions, two parts of horizontal flame regions exist, i.e. the upstream region and downstream region. The characteristic relative velocity could be estimated using:

$$\left|u_{ds}+u_l\right| \propto H_{ef}^{1/2}, \qquad \left|u_{us}+u_l\right| \propto H_{ef}^{1/2} \tag{A.14}$$

The combustion in the vertical flame region is also considered as being limited and thus ignored as a first approximation.

For a slightly higher ventilation velocity, e.g. 1.5 m/s, the length of the upstream flame and the backlayering is short, and therefore the entrained air in the upstream flame region will only be slightly vitiated (inerted). However, the air could be highly vitiated in the downstream flame region. If no dominating ventilation direction exists, the fresh air will be entrained from both sides of the tunnel by thermal pressure created by the hot smoke. The air entrained into the flame region on both upstream and downstream sides could be highly vitiated, see Figure 44. This phenomenon has not been clearly understood and needs to be further investigated. As a first approximation, the oxygen concentration will be implicitly accounted for in the following analysis. Therefore we have:

$$L_{f,tot} = L_{f,ds} + L_{f,us} = \frac{\dot{Q}-\dot{Q}_v}{\xi\beta\rho_o W\bar{Y}_{O_2}\Delta H_{O2} H_{ef}^{1/2}} \tag{A.15}$$

where $\bar{Y}_{O_2}$ is the average oxygen concentration of the entrained air, $L_{f,tot}$ is the total flame length (m).

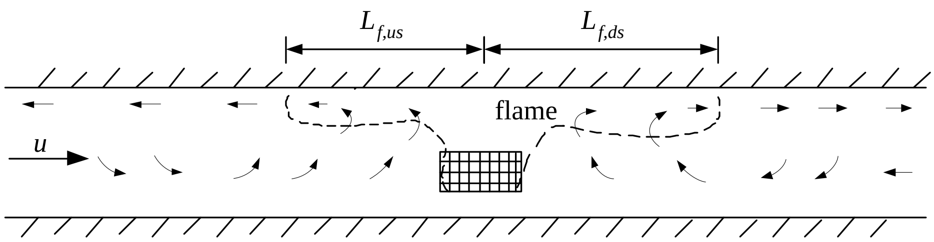

Figure 44 A schematic diagram of the vitiated gas entrained into the ceiling flame region under natural ventilation or low ventilation.

10 Appendix B – Theoretical model of ceiling gas velocity

10.1 Natural ventilation

A simplified model is applied here to investigate the ceiling gas velocity. Some assumptions are made here:

(1) The flow is one dimensional;
(2) The temperature profile is top hat, i.e. temperature is uniform at one cross section of different heights;
(3) The velocity profile is top hat, i.e. temperature is uniform at one cross section of different heights;
(4) The static pressure rise due to thermal expansion is limited and negligible.

For fires under natural ventilation, the momentum equation for one-dimensional smoke flow can be expressed as:

$$\frac{\partial}{\partial x}(\rho u^2 A) - \frac{\partial}{\partial x}(\frac{1}{2}\Delta\rho g h A) = -\frac{1}{2}C_{sf}\rho u^2 w_p \qquad \text{(B.1)}$$

where A is the cross-sectional area of smoke flow (m^2), t is time (s), x is distance along tunnel length axis (m), h is smoke layer depth (m), h_t is total heat transfer coefficient (kW/m^{2}K), w_p is wet perimenter of smoke layer (m), C_{sf} is the skin friction coefficient.

By neglecting the friction loss term on the right hand side, the above equation is transformed into:

$$\frac{\partial}{\partial x}(\rho u^2 A) = \frac{\partial}{\partial x}(\frac{1}{2}\Delta\rho g h A) \qquad \text{(B.2)}$$

At first we analyse the velocity at the smoke front. By integrating the momentum equation within a small range at the smoke front, it gives

$$\rho u^2 = \frac{1}{2}\Delta\rho g h \qquad \text{(B.3)}$$

The average velocity of the smoke front can therefore be expressed by:

$$u_g = 0.72\sqrt{g h_g \frac{\Delta T_g}{T_o}} \qquad \text{(B.4)}$$

Note that this equation is closely the same as that proposed by Bailey et al. [37]. This can be considered as the general equation for velocity of smoke front of a buoyancy-driven channel flow. Note that for pure gravity flow the corresponding equation is $u = \sqrt{gh}$.

For the initial condition of the ceiling jet, the momentum equation indicates that the changes in momentum is proportional to changes in buoyancy force. It could still be expected that the formulation of the gas velocity at the initial location is approximately the same as that for the smoke front, which is expressed as follows:

$$u_g \propto \sqrt{g h_g \frac{\Delta T_g}{T_o}} \tag{B.5}$$

Note that from the momentum equation of the vertical fire plume, a similar equation can be obtained.

Alpert's work [15] showed that the smoke layer height in the impingement region is proportional to the clearance height above the fire. Based on Alpert's work [15], Kunsch [38] obtained the initial smoke layer height for the one dimensional flow in a corridor under natural ventilation, i.e., :

$$h_g \propto \frac{H_{ef}^2}{W} \tag{B.6}$$

By introducing this term into the equation for gas velocity, we have:

$$u_g \propto \sqrt{g \frac{H_{ef}^2}{W} \frac{\Delta T_g}{T_o}} \tag{B.7}$$

According to Li et al's study [8-10], under natural ventilation (i.e. low velocity $V' < 0.19$), the maximum ceiling excess gas temperature in a tunnel fire can be expressed as:

$$\Delta T_g = 17.5 \frac{Q^{2/3}}{H_{ef}^{5/3}} \tag{B.8}$$

The gas velocity for the initial ceiling jet can therefore be expressed as follows:

$$u_g = C\left(\frac{H_{ef}}{W}\right)^{1/2}\left(\frac{Q}{H_{ef}}\right)^{1/3} \tag{B.9}$$

where C is a correction factor.

Although by theory the above temperature equation works only for gas temperatures lower than the possibly maximum ceiling gas temperature (approx. 1350 °C), it is assumed here that the above equation for gas velocity works in all the range, for simplicity.

10.2 Forced ventilation

By use of the same assumptions as for natural ventilation, the momentum equation for one-dimensional smoke flow in case of a fire under forced ventilation can be expressed as:

$$\frac{\partial}{\partial x}(\rho u^2 A) - \frac{\partial}{\partial x}\left(\frac{1}{2}\Delta\rho g h A\right) = -\frac{1}{2} C_{sf} \rho u^2 w_p - \frac{\partial (pA)}{\partial x} \tag{B.10}$$

Note that the pressure term on the right hand side, $-\partial(pA)/\partial x$, is positive for smoke flow towards downstream while negative for smoke reverse flow towards upstream. This indicates the ventilation system has different influences on the momentums of the downstream smoke flows and the upstream flow. Upstream of the fire, both the pressure term and pressure loss term results in more rapid decreases in the momentum of the smoke reverse flow.

For simplicity, let us focus on a small gas volume nearby the upstream boundary of the fire plumes and close to the ceiling. At this position the total pressure caused by the wind is approximately equivalent to the dynamic pressure of the wind. For the small smoke volume flowing from this location to the position of the maximum ceiling temperature (with a thickness of *h*), the Bernoulli equation can be approximately expressed as:

$$p_o + \rho_o gh + \frac{1}{2}\rho_o u_o^2 = p_g + \rho gh + \frac{1}{2}\rho u^2 + \Delta p_{loss} \qquad \text{(B.11)}$$

Note that the reference point for the hydrostatic pressure has been chosen to be the bottom of the ceiling jet. Note that the thickness of the initial ceiling jet is not a great value. It could be expected that under strong forced ventilation the hydrostatic pressure plays a much less important role compared to the dynamic pressure term, and thus ignored in the following. Further, as the distance is short, the pressure loss term is assumed to be negligible. Therefore, the above equation indicates:

$$\frac{1}{2}\rho_o u_o^2 = \frac{1}{2}\rho u^2 \qquad \text{(B.12)}$$

The above equation can also be obtained by applying the momentum equation to the small gas volume based on the same assumptions.

The initial ceiling jet velocity, u_g, can therefore be expressed as:

$$u_g = u_o\sqrt{1 + \frac{\Delta T_{\max}}{T_o}} \qquad \text{(B.13)}$$

This indicates that the initial ceiling jet velocity is proportional to the ventilation velocity and increases with the ceiling gas temperature.

11 Appendix C – Theoretical model of ceiling jet temperature

11.1 Small fires

First, let us carry out a theoretical analysis of the stratified smoke flows in the upper layer at a quasi-steady state. A schematic view of smoke spread upstream and downstream of the fire is shown in Figure 45. Similar to the vertical plume entrainment, it can be assumed that the entrainment velocity is proportional to the relative velocity of the smoke flow.

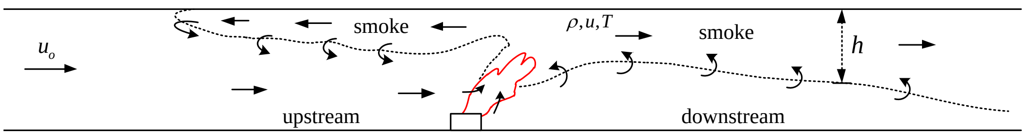

Figure 45 A schematic diagram of smoke spread upstream and downstream of the fire.

Downstream of the fire, the smoke flow at the upper layer entrains the air from the lower layer. Assuming that no heat source is introduced into the ceiling smoke flow (no combustion in the ceiling flow), the mass and energy equations can be expressed as:

$$\frac{\mathrm{d}}{\mathrm{d}\,x}(\rho u A) = \rho_o W v_e \qquad \text{(C.1)}$$

$$\frac{\mathrm{d}}{\mathrm{d}\,x}(\rho A u c_p T) = \rho_o W v_e c_p T_o - h_t w_p (T - T_o) \qquad \text{(C.2)}$$

The entrainment velocity, v_e (m/s), for downstream smoke flow could be expressed as:

$$v_e = \beta (u - u_l) \qquad \text{(C.3)}$$

In the above equations, u is smoke velocity (m/s), u_l is lower layer air velocity (m/s), A is cross-sectional area of the smoke flow (m^2), W is tunnel width at the bottom of the smoke layer (m), h_t is the total net heat transfer coefficient on tunnel walls (kW/m^{2}K), w_p is the wet perimeter of the smoke flow (M), β is the entrainment coefficient, ρ and T are average density (kg/m^3) and temperature of the smoke flow (K).

It is known that the dominating term in the differential energy equation, i.e. Eq. (29), is the heat loss to the tunnel structure. Therefore the effect of entrainment on the energy equation is ignored while solving the differential equations. To obtain an analytical solution, it is also assumed that the net heat transfer coefficient, h_t, and wet perimeter, w_p, (or the term $h_t w_p$) are constant. Therefore, we have:

$$\frac{\Delta T(x)}{\Delta T_{\max}} = \exp\left(-\frac{h_t w_p + \rho_o v_e W c_p}{\rho u A c_p} x\right) \qquad \text{(C.4)}$$

The above equation can be approximately expressed as:

$$\frac{\Delta T}{\Delta T_{\max}} \approx \exp(-a\frac{x}{H}) \tag{C.5}$$

For rectangular cross sections (A=hW), the dimensionless parameter a in the above equation can be expressed as:

$$a = \frac{h_t(H/h + 2H/W) + \rho_o v_e c_p H/h}{\rho u c_p} \propto \frac{h_t}{\rho u c_p} \tag{C.6}$$

where x is distance from the fire source (m) and h is the smoke layer height (m). Note that the smoke layer height is generally much smaller than the width and also the ratio h/W varies in a narrow range.

This suggests that the ceiling gas temperature varies as an exponential equation of the dimensionless distance from the fire if the parameter a is constant.

Upstream of the fire, the behavior of smoke flow is slightly different from that downstream of the fire. The fresh air flow at a high velocity could be considered to entrain the smoke from the upper layer and blow it away from the fire. In the case that the fresh air flow has a great enough velocity, it could arrest the smoke front and prevent any further spread, see Figure 45. Close to this point, the mass flow rate of the smoke flow decreases to 0. Assuming that no heat source is introduced into the horizontal smoke flow, the mass and energy equation can be expressed as:

$$\frac{\mathrm{d}}{\mathrm{d}x}(\rho u A) = -\rho W v_e \tag{C.7}$$

$$\frac{\mathrm{d}}{\mathrm{d}x}(\rho A u c_p T) = -\rho W v_e c_p T - h_t w_p (T - T_w) \tag{C.8}$$

The entrainment velocity for the upstream smoke flow could be expressed as:

$$v_e = \beta(u + u_l) \tag{C.9}$$

Similar to the treatment to the downstream smoke flow, the analytical solution can be expressed as follows:

$$\frac{\Delta T}{\Delta T_{\max}} = \exp(-\frac{h_t w_p}{\rho A u c_p} x) \tag{C.10}$$

The above equation can then be simplified into:

$$\frac{\Delta T}{\Delta T_{\max}} = \exp(-b\frac{x}{H}) \tag{C.11}$$

where, for rectangular cross sections, the dimensionless parameter, b, is defined as:

$$b = \frac{h_t(H/h + 2H/W)}{\rho u c_p} \propto \frac{h_t}{\rho u c_p} \tag{C.12}$$

From the above analysis, it is expected that for smoke flows both downstream and upstream of the fire, the temperature distribution can be approximated using an exponential function.

Note that the Stanton number St is correlated with the skin friction coefficient, which can expressed approximately as follows:

$$\mathrm{St} = \frac{h_c}{\rho u c_p} = \frac{1}{2} C_f \tag{C.13}$$

where h_c is the convective heat transfer coefficient (kW/m^{2}K), C_f is the friction coefficient. This suggests that for small fires where the convective heat transfer dominates, the decrease of the ceiling gas temperature follows an exponential equation. However, the heat transfer coefficient in Eq. (31) and Eq. (37) is the total heat transfer coefficient on a tunnel wall, h_t, rather than the convective heat transfer coefficient, h_c. For most tunnel fires that are relevant, the radiative heat transfer dominates heat transfer to the tunnel walls in the near field of the fire source. In such cases, the term in the numerator of a and b should be $2+2h/W$ instead of $1+2h/W$. In reality, the conductive heat transfer plays an important role in the total heat transfer from hot gases to the tunnel wall, and its importance increases with time. In other words, at the early stages of a fire, the conduction has an insignificant influence on the heat transfer but the importance of the heat conduction increases with time.

Therefore, the total heat transfer coefficient is not constant along the tunnel. Instead, it should be greater close to the fire but less far away from the fire. Similarly it should be greater at the early stage of the fire and less as time goes on. If the tunnel walls are exposed to hot gases for a long time, heat conduction will dominate the heat transfer, and then the coefficient approaches a constant along the tunnel. Despite this, based on the test data, it has been found that the ceiling temperature distribution along the tunnel can be well represented by the sum of two exponential equations, and the tunnel height could be used to represent the smoke layer height, h. This is in good correlation to the theory, i.e. Eq. (32) and Eq. (38).

11.2 Large fires

When significant combustion occurs beneath the ceiling, the energy equation need to add the heat source terms:

$$\frac{\mathrm{d}}{\mathrm{d}x}(\rho A u c_p T) = \rho_o W v_e c_p T_o - h_t w_p (T - T_o) + \frac{\partial Q}{\partial x} \tag{C.14}$$

The positive heat source term indicates that the smoke temperature decreases more slowly with distance from the fire, and the temperature could even increase during certain ranges.

12 Appendix D – Theoretical model of smoke radiation

The total net heat flux on a surface is the sum of convective heat flux and radiative heat flux, which can simply be expressed as:

$$\dot{q}''_{net} = \dot{q}''_{net,c} + \dot{q}''_{net,r} \tag{D.1}$$

In large tunnel fires, generally the radiative heat flux is much higher than the convective heat flux. Also, note that the convective heat flux can be easily calculated using the equations proposed in the previous section. Therefore the calculation of the radiative heat flux is the focus of the following sections.

12.1 Exposed tunnel ceiling and walls at upper layer

The surfaces at the upper layer are surrounded by smoky gases or flames in a large fire. The emissivity of the walls is assumed to be close to 1. Further, the view factor between the smoke and ceiling or walls can also be assumed to be 1. This is suitable for large fires but for small fires these assumptions can result in a conservative estimation. The net radiative heat flux can then be estimated using:

$$\dot{q}''_{net,w} = \frac{\dot{Q}_{g-w}}{A_w} = \frac{(e_{b,g} - e_{b,w})/A_w}{(1-\varepsilon_g)/(\varepsilon_g A_g) + 1/A_w F_{w-g} + (1-\varepsilon_w)/(\varepsilon_w A_w)} \tag{D.2}$$

where the subscript w indicates wall and g indicates hot gases.
Note that for A_w=A_g and F_{o-g}=1, we have:

$$\dot{q}''_{net,w} = \frac{e_{b,g} - e_{b,w}}{1/\varepsilon_g + (1-\varepsilon_w)/\varepsilon_w} \tag{D.3}$$

The incident heat flux received at the ceiling or wall surfaces can be estimated by:

$$\dot{q}''_{inc,w} = \frac{\dot{q}''_{net,w}}{\varepsilon_w} + e_{b,w} = \frac{\sigma(T_g^4 - T_w^4)}{\varepsilon_w/\varepsilon_g + 1 - \varepsilon_w} + \sigma T_w^4 \tag{D.4}$$

Given that the emissivity of the wall and the objects normally ranges from 0.85 to 0.95, an emissivity of 1 for the ceiling and upper walls can be assumed. Therefore, the incident heat flux at the upper layer can be simply written in the following form:

$$\dot{q}''_{inc,w} \approx \varepsilon_g \sigma T_g^4 \tag{D.5}$$

For large tunnel fires, the gas emissivity, ε_g, approaches 1.

12.2 Heat flux in lower layer

12.2.1 Horizontal and vertical object surfaces

The smoke flow in a tunnel fire is sometimes divided into two layers, i.e. a relatively hot upper layer and a relatively cool lower layer. There is always temperature stratification, even in well mixed conditions at a position far away from the fire. The heat flux to an object in the lower layer is mainly attributed to the radiation from upper-layer hot gases. Note that the gas temperature does not vary significantly along the length of a tunnel section of two or three times the tunnel height. Therefore, a three-dimensional radiation problem can be simplified into a two-dimensional problem. The radiation surfaces can be divided into three types, i.e. hot gas surface in the upper layer (*g*), object in the tunnel (*o*), and cold walls and floors in the lower layer (*w*). A diagram of surface radiation to an object in the lower layer is shown in Figure 46. Note that the hot gases surrounded by the upper tunnel walls as a whole are considered as one surface in Figure 46.

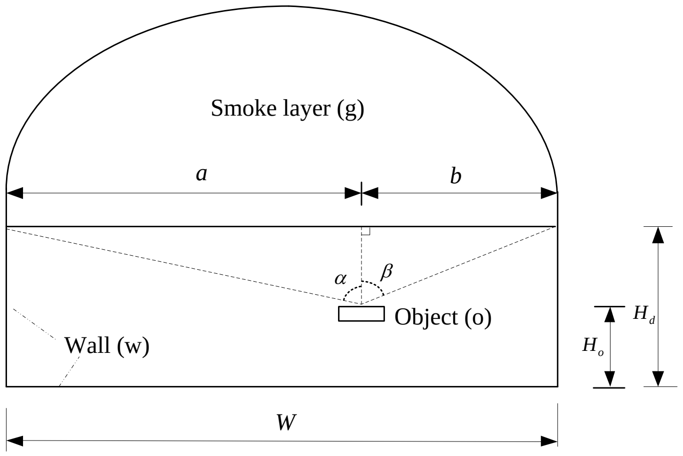

Figure *46* *A diagram of radiation to an object at the lower layer.*

Note that the radiation between the object and the lower wall is limited compared to the radiation emitted from the hot gases. We may assume $e_{b,w} \approx e_{b,o}$. The radiation to an object in the lower layer can be represented by an electrical circuit analog as shown in Figure 47.

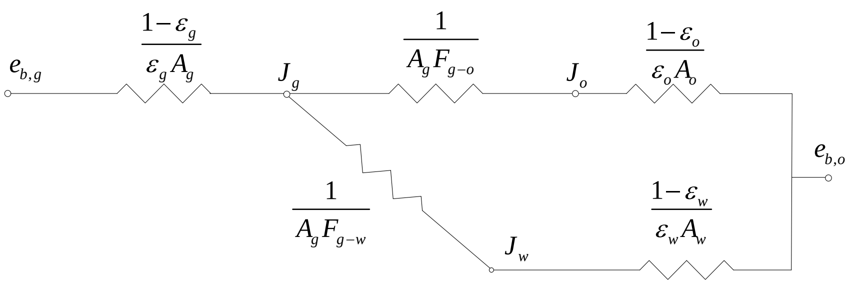

Figure *47* *Electrical circuit analog of radiation to an object in the lower layer.*

The view factor from the gas to the wall $F_{g\text{-}w}$ is much larger than the view factor from the gas to the object $F_{g\text{-}o}$, therefore the most of the heat goes to the wall. Thus the heat flux to object can be expressed as:

$$\dot{Q}_{net,g-o} = \frac{\dfrac{1}{F_{g-w}A_g} + \dfrac{1-\varepsilon_w}{\varepsilon_w A_w}}{\dfrac{1}{F_{g-o}A_g} + \dfrac{1-\varepsilon_o}{\varepsilon_o A_o}} \frac{e_{b,g} - e_{b,o}}{\dfrac{1-\varepsilon_g}{\varepsilon_g A_g} + \dfrac{1}{F_{g-w}A_g} + \dfrac{1-\varepsilon_w}{\varepsilon_w A_w}} \tag{D.6}$$

Note that $F_{g\text{-}w}$=1 but $F_{w\text{-}g}\neq 1$, and $F_{g\text{-}o}A_g = F_{o\text{-}g}A_o$. The radiation heat flux from the smoke layer to the object can be expressed as:

$$\dot{q}''_{net,g-o} = \frac{\dot{Q}_{net,g-o}}{A_o} = \left(\frac{\frac{1}{A_g} + \frac{1-\varepsilon_w}{\varepsilon_w A_w}}{\frac{1}{\varepsilon_g}\frac{1}{A_g} + \frac{1-\varepsilon_w}{\varepsilon_w A_w}}\right)\frac{e_{b,g} - e_{b,o}}{\frac{1}{F_{o-g}} + \frac{1}{\varepsilon_o} - 1} \qquad \text{(D.7)}$$

Recall most of the radiation to the object comes from the smoke layer beside the object within a tunnel length of two or three tunnel heights, and the gas temperature within this range does not vary significantly. Therefore the characteristic radiation temperature can be considered constant. By considering a longitudinal length of dx (m), we know the exposed area for the smoke layer, A_g (m^2), and the lower layer, A_w (m^2):

$$A_g = Wdx \qquad \text{(D.8)}$$

$$A_w = (W + 2H_d)dx = P_w dx \qquad \text{(D.9)}$$

Therefore, the equation for net heat flux from the smoke layer to the object surface can be simplified to:

$$\dot{q}''_{net,g-o} = C_{r1}C_{r2}\sigma(T_g^4 - T_o^4) \qquad \text{(D.10)}$$

where coefficients C_{r1} and C_{r2} are defined as:

$$C_{r1} = \left(\frac{\frac{1}{W} + \frac{1-\varepsilon_w}{\varepsilon_w P_w}}{\frac{1}{\varepsilon_g W} + \frac{1-\varepsilon_w}{\varepsilon_w P_w}}\right) \approx \varepsilon_g\,,\; C_{r2} = \frac{\varepsilon_o F_{o-g}}{\varepsilon_o + (1-\varepsilon_o)F_{o-g}}$$

The incident heat flux can be estimated using:

$$\dot{q}''_{inc,o} = \frac{\dot{q}''_{net,g-o} + \dot{q}''_{net,w-o}}{\varepsilon_o} + e_{b,o} \qquad \text{(D.11)}$$

The radiation between the object and the walls is limited, i.e. the net heat flux between the walls and object is much smaller than the heat flux between the gas and object. Therefore Eq. (D.11) can be written as:

$$\dot{q}''_{inc,o} = C_{r1}C_{r2}\sigma(T_g^4 - T_o^4)/\varepsilon_o + \sigma T_o^4 \qquad \text{(D.12)}$$

The above equations can further be simplified, given that the emissivity of the wall and the object normally ranges from 0.85 to 0.95 with an average value of 0.9. In such cases, C_{r1} is nearly the same as ε_g and C_{r2} is approximately the same as $0.9F_{o\text{-}g}$. Using these assumptions, the net heat flux on the target surface can now be expressed in the following equation:

$$\dot{q}''_{net,o} = \dot{q}''_{net,g-o} \approx 0.9\varepsilon_g F_{o-g}\sigma(T_g^4 - T_o^4) \qquad \text{(D.13)}$$

Given that the temperature of the object surface is generally much lower than the smoke layer temperature, the incident heat flux received on the object surface can be simplified to:

$$\dot{q}''_{inc,o} \approx \varepsilon_g F_{o-g} \sigma T_g^4 \qquad \text{(D.14)}$$

When the object is immersed in the smoke layer, the view factor equals 1 and the above equation becomes the same equation as that for exposed tunnel ceiling and walls at upper layer. As a rough estimation, the height of a characteristic smoke layer can be set at 50 % of the tunnel height, unless information indicating a better estimation is available. This assumption could work well if the ceiling gas temperature is used as the characteristic temperature of the smoke layer.

The emissivity depends on local soot concentrations which is dependent on the soot production of the fire. Usually this term is difficult to determine. The smoke layer can be considered as optically thick in most tunnel fires, indicating that the emissivity approaches 1. In large tunnel fires, it is certain that the emissivity can be considered as 1. In a small fire or at the early stage of a large fire, the emissivity is much lower. However, over time the upper wall surface temperature approaches the gas temperature even for a small fire, e.g. a 5 MW fire with relatively low ceiling height, or for a tunnel with fire protection linings. The emissivity in the above equations in reality is a property of the whole upper smoke layer including the tunnel ceiling and walls surrounded by the smoke (major effects), and also the walls and floors below the smoke layer (minor effects). In thermally thin cases most of the radiation from the upper ceiling and walls will be emitted to the lower layer as the radiation absorbed by smoke could be limited. Therefore, the emissivity of the whole upper layer is slightly higher than what would be expected. In summary, the total emissivity of the upper layer can also be assumed to be 1 in such cases, although it could result in a slightly conservative estimation.

Therefore, the main parameter that must be determined is the view factor from the object to the smoke layer, which will be discussed in the following text for different placements of the object.

View Factors in tunnels

For an object on the tunnel floor or a certain height above the floor with its surface facing upward, the view factor can be calculated using:

$$F_{o-g} = \frac{1}{2}(\sin\alpha + \sin\beta) \qquad \text{(D.15)}$$

where α and β are the angles plotted in Figure 46.

The object could also be placed on the wall with its surface facing the opposite wall, e.g. placed on the right wall in Figure 46, in which case the view factor can be calculated using:

$$F_{o-g} = \frac{1}{2}(1 - \cos\alpha) \qquad \text{(D.16)}$$

If the object is placed on the left wall in Figure 46, the angle in the above equation should be β instead of α.

If the object surface is facing one side of the tunnel, the view factor can be estimated by:

$$F_{o-g} = \frac{1}{2\pi}(\alpha+\beta) = \frac{1}{2\pi}[\tan^{-1}(\frac{a}{H_d - H_o}) + \tan^{-1}(\frac{b}{H_d - H_o})] \qquad \text{(D.17)}$$

where H_d-H_o is the distance between the hot layer and the object surface center, *a* and *b* are the horizontal distances between the target center and the side walls, see Figure 46.

When the object is surrounded by hot gas having a characteristic gas temperature, the view factor is close to 1, especially if the object's surface is facing upward. Recall the smoke layer height can be estimated as 50 % of tunnel height. One reason for this assumption is that ceiling gas temperature is used as the characteristic gas temperature in the calculation of the heat flux. In reality, there always exists a temperature difference between upper gas layer and lower floor layer even when the so-called smoke de-stratification has occurred. Therefore, the decrease of view factor somewhat compensates for the probable overestimation of the characteristic gas temperature.

The key parameters in the heat flux equation, e.g. C_{r1} and C_{r2}, are dimensionless and are not sensitive to tunnel geometry. This insensitivity indicates that the model is mainly related to the shape of the lower floor layer and the position of the object. Therefore, it is suitable for tunnels with different geometries.

The proposed equation can be used to estimate heat fluxes received by evacuees, firefighters, or neighboring vehicles in case of a tunnel fire. Further, it can be used to estimate the possibility of fire spread to neighboring vehicles or other objects.

12.2.2 Inclined target surfaces

In some cases, the surface is neither horizontal nor vertical, as shown in Figure 48. There can be an inclination angle between the object surface and smoke layer surface. If such an inclined surface is in the vicinity of the fire source, the flames can also contribute to the heat radiation to the surface. Therefore, the total heat flux received on the surface should consist of both the smoke layer and the fire source. In this section we only discuss the heat flux from smoke layer; the flame radiation will be described in Sect. 10.7.3.

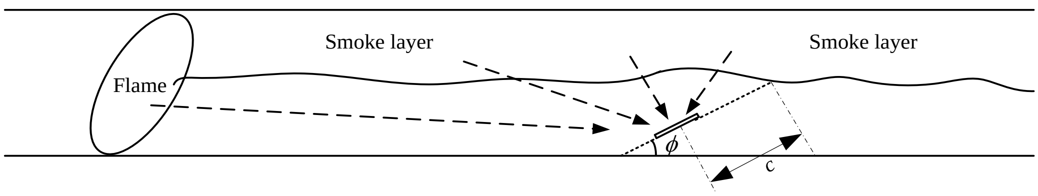

Figure 48 A diagram of radiation from flame and smoke layer to the object.

In calculation of heat fluxes received by inclined surfaces, the effect of inclination must be accounted for. The model for estimation of view factor from rectangular radiators to differential areas at various plane angles can be used here, see Figure 49. The object lies on a plane normal to the line of intersection between the planes with its origin at one corner of the rectangle.

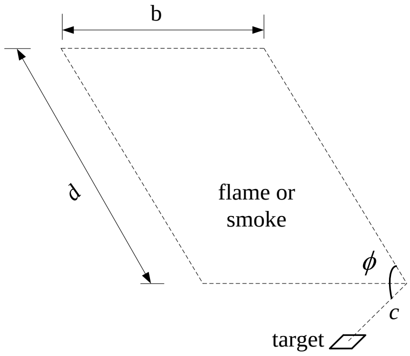

Figure 49 A diagram of radiation from flame and smoke layer to the object.

The radiation from the rectangular radiator to the object can be expressed using the view factor, $F_{o\text{-}radiator}$ or $F_{o\text{-}g}$, which is given in the following equation [39, 40]:

$$F_{o-radiator} = \frac{1}{2\pi}\left\{\tan^{-1}\left(\frac{1}{L}\right) + V(N\cos\phi - L)\tan^{-1}(V) + \frac{\cos\phi}{W}\left[\tan^{-1}\left(\frac{N - L\cos\phi}{W}\right) + \tan^{-1}\left(\frac{L\cos\phi}{W}\right)\right]\right\} \quad \text{(D.18)}$$

where

$$V = \frac{1}{\sqrt{N^2 + L^2 - 2NL\cos\phi}}$$

$$W = \sqrt{1 + L^2\sin^2\phi}$$

$$N = \frac{d}{b}$$

$$L = \frac{c}{b}$$

In the above equation, b and d are side lengths of the radiator (m), c is the distance from the object to the intersection line of the two planes (m), and ϕ is the angle between the two planes (°).

The angle can vary between 0 and 180°. Note that when the angle approaches 0 or 180°, numerical instabilities could result in unreasonable value for the view factor. Therefore it should be kept in mind that the overall view factor obtained from a calculation should never be less than 0 or greater than 1.

Eq. (D.18) can be used to estimate the heat fluxes from both the vertical flame and the smoke layer to an inclined surface.

For radiation from the smoke layer which can be considered as an infinitely long plate above the object, Eq. (D.18) can be simplified into:

$$F_{o-radiator} = \frac{1}{2\pi}\left\{\tan^{-1}\left(\frac{1}{L}\right) + \frac{\cos\phi}{W}\left[\frac{\pi}{2} + \tan^{-1}\left(\frac{L\cos\phi}{W}\right)\right]\right\} \quad \text{(D.19)}$$

In the above equation, the parameter *a* has been eliminated. Therefore the view factor is only a function of *b*, *c* and angle ϕ. For an object placed at the centerline of the tunnel, radiation from two radiation planes to the object must be summed, i.e.

$$F_{o-g} = F_{o-g,1} + F_{o-g,2} \quad \text{(D.20)}$$

For each radiation plane, the equation for an infinitely long plate is used. The only difference in calculation of the two view factors is the parameter *b*. The sum of this parameter, *b*, for these two view factors should be equal to the tunnel width.

12.2.3 Radiation from vertical flames in large tunnel fires

For a large tunnel fire, people (such as firefighters) located upstream of the fire can see the flame occupying the whole tunnel cross-section at the fire site, see Figure 50. Here the radiation from the vertical part of the flames is discussed.

The incident radiative heat flux received by the person at *L* meters away from the fire can be estimated using the following equation:

$$\dot{q}''_{inc,F-o} \approx \varepsilon_F \sigma T_F^4 F_{o-F} \quad \text{(D.21)}$$

In most cases, especially for a large fire, the emissivity of the flame is approximately 1, i.e. ε_F=1. The average flame temperature can be assumed to be between 1000 ^oC and 1100 ^oC.

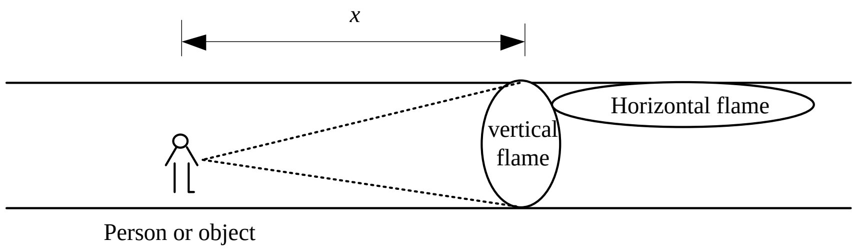

Figure 50 A diagram of flame radiation to an object in a large tunnel fire

The flame can be considered as a radiating plane by a person some distance away from the fire. This plane can be divided into four parts, as shown in Figure 51. The four areas plotted in the figure correspond to the part of flame which is visible to the object located either upstream or downstream. The areas correspond to the whole tunnel cross-sectional area only if there is no smoke along the path, e.g. the backlayering has been prevented by forced flows.

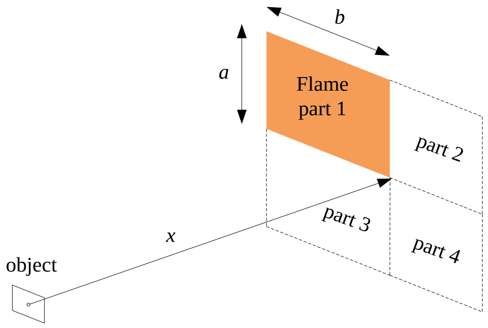

Figure 51 A diagram of view factor between the object and the flame plane.

Note that the total view factor is the sum of the four parts, i.e.

$$F_{o-F} = \sum_{i=1}^{4} F_{o-F,i} = F_{o-F,1} + F_{o-F,2} + F_{o-F,3} + F_{o-F,4} \qquad \text{(D.22)}$$

where the view factor, $F_{o\text{-}F}$, for flame part 1 is:

$$F_{o-F,1} = \frac{1}{2\pi}\left[\frac{a}{\sqrt{a^2+x^2}}\tan^{-1}\left(\frac{b}{\sqrt{a^2+x^2}}\right) + \frac{b}{\sqrt{b^2+x^2}}\tan^{-1}\left(\frac{a}{\sqrt{b^2+x^2}}\right)\right]$$

where *a* and *b* are dimensions (m) of part 1 of the flame (see Figure 51) , and *x* is the distance between object and the flame (m). The arctan function is represented by $\tan^{-1}$. For a smaller fire, the area, A_T, can be replaced by the estimated flame area having a line of sight to the object. However, the point source method is recommended for estimation of radiation from a small tunnel fire.

Eq. (D.22) suggests that for a very large tunnel fire, i.e. a significant horizontal flame exists, the heat flux received at a certain distance increases with the tunnel cross-sectional area. In comparison, the heat radiation in a small fire can be assumed to be independent of the tunnel width.

For an inclined surface, e.g. Figure 48, the actual heat flux from the flame to the object surface is reduced as follows:

$$\dot{q}''_{inc,F} = \dot{q}''_{inc,F,vertical}\cos\beta \qquad \text{(D.23)}$$

where $\dot{q}''_{inc,F,vertical}$ is the incident heat flux received at a vertical surface facing the flame (kW/m^2), and β is the angle between the radiation and the normal line of the object surface (°).

SP Technical Research Institute of Sweden

Our work is concentrated on innovation and the development of value-adding technology. Using Sweden's most extensive and advanced resources for technical evaluation, measurement technology, research and development, we make an important contribution to the competitiveness and sustainable development of industry. Research is carried out in close conjunction with universities and institutes of technology, to the benefit of a customer base of about 10000 organisations, ranging from start-up companies developing new technologies or new ideas to international groups.

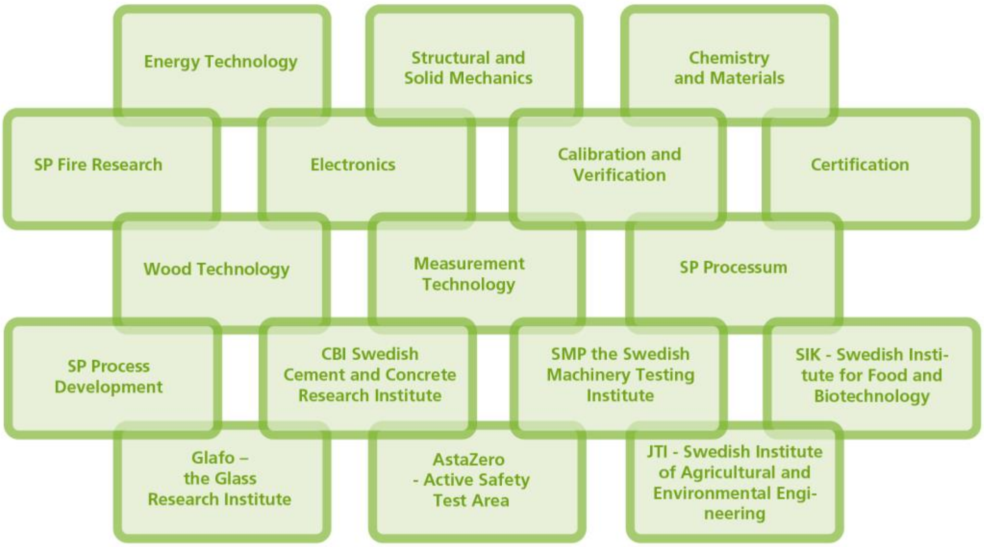

SP Technical Research Institute of Sweden

Box 857, SE-501 15 BORÅS, SWEDEN

Telephone: +46 10 516 50 00, Telefax: +46 33 13 55 02

E-mail: info@sp.se, Internet: www.sp.se

www.sp.se

Fire Research

SP Report 2015:23

ISBN 978-91-88001-53-5

ISSN 0284-5172

More information about publications published by SP: **www.sp.se/publ**